Fusion Engineering and Design 112 (2016) 102–116

Contents lists available at ScienceDirect

Fusion Engineering and Design

journal homepage: www.elsevier.com/locate/fusengdes

Thermodynamic model for grain boundary effects on hydrogen solubility, diffusivity and permeability in poly-crystalline tungsten

Takuji Oda

Department of Nuclear Engineering, Seoul National University, 1 Gwanak-ro, Gwanak-gu, Seoul 151-742, South Korea

HIGHLIGHTS

- A thermodynamic model to simulate grain boundary effects on hydrogen behaviors in poly-crystalline W was established.
- With this model, the effective solubility, diffusivity and permeability of hydrogen are calculated as a function of grain size.
- Grain boundary significantly change the hydrogen behaviors in poly-crystalline W up to around 1000 K.

ARTICLE INFO

Article history:
Received 6 March 2016
Received in revised form 27 July 2016
Accepted 3 August 2016
Available online 10 August 2016

Keywords:
Hydrogen
Tungsten
Grain boundary
Solubility
Diffusivity
Permeability

ABSTRACT

A thermodynamic model to evaluate effects of grain boundary (GB) on hydrogen behaviors in poly-crystalline tungsten is established. With this model, the effective solubility, diffusivity and permeability of hydrogen in tungsten equilibrated with surrounding H_2 gas can be calculated as a function of grain size, temperature and H_2 partial pressure. By setting 1.0 eV to the binding energy of hydrogen to GBs and 0.4 eV to the diffusion barrier of hydrogen along GBs, the model reasonably reproduces some experimental data on the effective diffusivity and permeability. Comparisons between calculation results by the model and available experimental data show that GBs significantly affect the hydrogen behaviors up to around 1000 K or higher in practical materials. Therefore, the effects of GBs need to be considered in analysis of experimental results, for which the present model can be utilized, and in prediction of tritium inventory and leakage in fusion reactors.

1. Introduction

Hydrogen solubility, diffusivity, and permeability in tungsten, a promising candidate material for plasma facing components (PFCs) in fusion reactors, are important thermodynamic properties for estimating the tritium inventory and leakage in/through PFCs. Many studies have been performed to evaluate these quantities [1,2]. Hydrogen behaviors in W are not so complicated if the crystal lattice is perfect. In practical materials, however, lattice defects are inevitably involved, and then the solution, diffusion and permeation behaviors of hydrogen largely change. Moreover, in nuclear fusion environment, radiation defects are expected to affect the hydrogen behaviors [3,4].

Lattice defects basically act as hydrogen traps in W, which increase the effective solubility and decrease the effective diffusivity of hydrogen. Many previous studies focused on mono-vacancy and examined its effects on the solution and diffusion behaviors of hydrogen in single-crystal W [5–12]. For example, it was shown that a mono-vacancy traps multiple H atoms in W: up to around 12 H atoms at 0 K [5,9,10] and up to around 6 H atoms at room temperature [9,10].

Dislocation [13], grain boundary (GB) [14–19] and some impurities [2,6,20–22] are also known to act as traps. In experiments on thermal desorption of hydrogen in W, a desorption peak related to intrinsic traps is usually observed. This peak indicates the existence of hydrogen trap to which the binding energy of hydrogen is, for example, 0.85 eV [23] and 0.7–0.9 eV [3] (which is obtained by subtracting a hydrogen diffusion barrier from a detrapping energy). However, it is difficult to assign this peak to a specific defect because several intrinsic traps such as dislocation, GB and impurities are likely to have the binding energies in around that energy range.

Among the lattice defects, GB has been attracting increasing attention due to the importance of GBs in fine-grain W materials [24,25], which are expected to bring improved mechanical properties. Several computational studies were performed to uncover GB effects on the hydrogen behaviors in atomic scale [14–18]. Specifically, two methods of atomistic simulations have been applied to

E-mail address: oda@snu.ac.kr

http://dx.doi.org/10.1016/j.fusengdes.2016.08.001
0920-3796/

study the GB effects. One is first-principles calculation based on density functional theory (DFT), and the other is classical molecular dynamics (MD) method with two bond-order potential (BOP) models parameterized by Juslin et al. [26] and Li et al. [27]. DFT calculation was used to evaluate the stability and the mobility at/around specific GBs, including Σ5 tilt GB [14], Σ3 tilt GB [15] and W(110)/W(112) interface [16], while MD simulation was employed to find general trends of hydrogen stability and mobility in systems containing various types of GBs [17,18].

Despite the accumulation of detailed information on the GB effects thanks to atomistic simulations, the information has not been effectively utilized to interpret and analyze experimental results. One of the reasons of this is that quantities that can be determined by atomistic simulation such as the binding energy of H atom to GB are not simply reflected in quantities that can be obtained by experiment such as effective hydrogen solubility. This is because apparent effects of GBs depend on several parameters including grain size, hydrogen concentration, temperature, etc. In the present study, therefore, in order to systematically relate these two types of quantities, a thermodynamic model is constructed. This model enables us to calculate the effective solubility, diffusivity and permeability of hydrogen in poly-crystalline bcc-W equilibrated with surrounding H_2 gas, as a function of grain size, temperature and partial pressure of H_2 in the gas phase.

The remaining part of the present paper is organized as follows. In Chapter 2, the framework of the thermodynamic model is introduced. The modeling procedure and the definition of model parameters are described. In Chapter 3, calculation results with the thermodynamic model on the effective solubility, diffusivity and permeability of hydrogen are presented with varying grain sizes. The calculation results are compared with available experimental data. In addition, since some model parameters involve non-negligible uncertainties at present, results of sensitivity analyses on such parameters are also provided. In Chapter 4, after discussing uncertainties in the model and model parameters, experimental studies that are expected to contribute to refining the model are suggested and implications to fusion engineering R&D are mentioned. Finally, the paper is closed with concluding remarks in Chapter 5.

2. Methods

In this chapter, first of all, effects of hydrogen traps in general are described in Section 2.1. Then, the scope and the target of the present model is explained in Section 2.2. A thermodynamic model based on the equilibrium theory is derived to achieve the target of the present study in Section 2.3. Model parameters are set in Section 2.4 based on consideration of the structure of poly-crystalline bcc-W and results of reported atomistic simulations. Subsequently, formulation for evaluation of effective hydrogen solubility, diffusivity and permeability is given in Section 2.5. Finally, after summarizing the concept and parameters of the model in Section 2.6, experimental data to compare with calculation results are introduced in Section 2.7.

2.1. Effects of hydrogen traps in general

Each trap has characteristic influence on hydrogen behavior. For hydrogen diffusion, the effective diffusivity (D_{eff}) can be approximated as the weighted sum over contributions of different hydrogen states under the assumption that diffusion between different states do not significantly contribute to D_{eff} [28]. In a poly-crystalline specimen containing various lattice defects, D_{eff} is written down as

$$D_{eff} = \sum_{i}^{all-states} f_i D_i = f_{H-lat} D_{H-lat} + f_{H-vac} D_{H-vac} + f_{H-GB} D_{H-GB} + f_{H-surf} D_{H-surf} + f_{H-dis} D_{H-dis} + \ldots, \quad (1)$$

$$\sum_{i}^{all-states} f_i = 1, \quad (2)$$

where f_i represents the fraction of H atoms of state-i to all H atoms in the specimen and D_i the diffusivity of H atoms of state-i. For examples, $f_{H\text{-}lat}$ and $D_{H\text{-}lat}$ are respectively the fraction of H atoms located in the lattice, which are tetrahedral interstitial sites in bcc-W, and the diffusivity of the H atoms in the lattice. $f_{H\text{-}vac}$ and $D_{H\text{-}vac}$ are respectively the fraction of H atoms trapped by vacancies and the diffusivity of the H atoms as V-H complexes. $f_{H\text{-}GB}$ and $D_{H\text{-}GB}$ are respectively the fraction of H atoms trapped by GBs and the diffusivity of the H atoms along GBs. Similarly, $f_{H\text{-}surf}$ and $D_{H\text{-}surf}$ are of H atoms located on surfaces, and $f_{H\text{-}dis}$ and $D_{H\text{-}dis}$ are of H atoms trapped by dislocations.

In order for H atoms of a certain state to have a significant contribution to D_{eff}, the product of f_i and D_i needs to be relatively large. For H atoms trapped by vacancies in W, for example, $f_{H\text{-}vac}$ is large due to the strong trap effect of vacancy, while $D_{H\text{-}vac}$ is small as the migration of V-H complexes involves the displacement of vacancy, which requires a large activation energy (1.78 eV [29]). Hence, whether $f_{H\text{-}vac}D_{H\text{-}vac}$ is significant or not is determined by balance between large $f_{H\text{-}vac}$ and small $D_{H\text{-}vac}$. In the case of hydrogen in bcc-Fe, in which V-H interaction is qualitatively similar to that in W [30], it was confirmed by MD simulation that $f_{H\text{-}vac}D_{H\text{-}vac}$ is much smaller than $f_{H\text{-}lat}D_{H\text{-}lat}$ [31]. It should be reasonable to assume that this relation is satisfied also in W based on the similarity on V-H interactions between bcc-Fe and W. Moreover, in thermal desorption experiments of hydrogen in W, rate models were often used to reproduce experimental results with assuming that V-H complexes were immobile [32,33]. This fact also indicates that the contribution of $f_{H\text{-}vac}D_{H\text{-}vac}$ is sufficiently small in W, although there has been no research that quantified $f_{H\text{-}vac}D_{H\text{-}vac}$ in W.

One of the important points regarding the trap effects in the effective diffusivity is that H atoms trapped by GBs, surfaces and dislocations can diffuse along/on them, while H atoms trapped by a deep trap like vacancy hardly diffuse until detrapping. Thus, we cannot neglect the contribution of H atoms trapped at GBs, surfaces and dislocations to the effective diffusivity of hydrogen. Regarding the surface effect, however, since the surface diffusion does not occur perpendicular to the surface, we can neglect it in most experimental settings. Note that the diffusion along GBs or along dislocations are rather isotropic because the networks of GBs and dislocations are almost uniformly spread over the system.

Consequently, if we take into account the five hydrogen states in W, namely H atoms at the lattice sites, at vacancies, at GBs, at surfaces and at dislocations, the effective diffusivity is approximately written as

$$D_{eff} \sim f_{H-lat} D_{H-lat} + f_{H-GB} D_{H-GB} + f_{H-dis} D_{H-dis}, \quad (3)$$

$$f_{H-lat} + f_{H-GB} + f_{H-vac} + f_{H-surf} + f_{H-dis} = 1, \quad (4)$$

Regarding trap effects in hydrogen solubility, the ratio of effective solubility (S_{eff}) to 'true' solubility (S_{true}), which is the solubility in a single-crystal specimen at the equilibrium state where defect concentrations are negligibly low, is expressed as

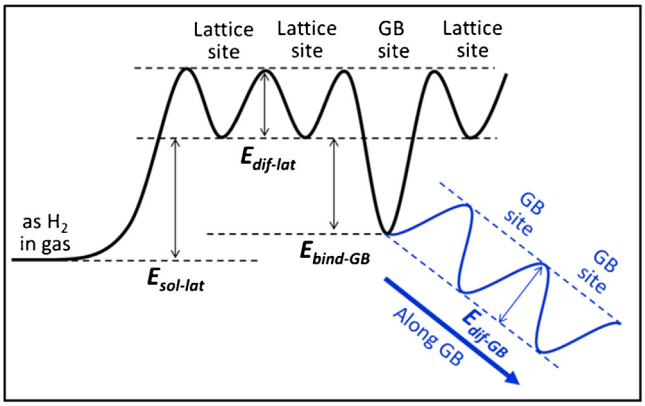

Fig. 1. Potential energy curve for H atom assumed in the present study.

$$\frac{S_{eff}}{S_{true}} \sim \frac{f_{H-lat}+f_{H-GB}+f_{H-vac}+f_{H-surf}+f_{H-dis}}{f_{H-lat}+f_{H-surf}} = \frac{1}{f_{H-lat}+f_{H-surf}}. \tag{5}$$

If the contribution of surfaces is negligibly small, Eq. (5) is approximately written as

$$\frac{S_{eff}}{S_{true}} \sim \frac{1}{f_{H-lat}}. \tag{6}$$

This condition seems to be satisfied in a previous research with a W cylinder sample of 3.17 cm diameter and 12.8 cm length at 8×10^4 Pa of H_2 gas pressure between 1120 and 2080 K [34], as Sieverts' law was satisfied and the activation energy of solubility (1.04 eV [34]) was consistent with the hydrogen solution energy in the lattice (around 1 eV in DFT calculation [7,35]), not with that on the surface (−0.91 eV in DFT calculation [36] and similar values in experiment [37,38]).

Regarding trap effects in hydrogen permeability, it can be surveyed by analyzing effective permeability of hydrogen, which is the product of effective diffusivity and effective solubility if surface processes are not rate-controlling processes in a hydrogen permeation phenomenon. This condition seems to be widely valid in W, as confirmed in the following conditions in previous experiments: a gas permeation experiment with 10^{-4}–200 Torr of H_2 atmosphere over 1050–2400 K [39], a gas permeation experiment with 10^4–10^5 Pa of H_2 and D_2 atmosphere over 720–850 K [40], and an ion driven permeation experiment of 1 keV T^+ irradiation with a flux of 9×10^{18} ions m^{-2} s^{-1} over around 550–650 K [41].

2.2. Scope of the present study

In the present study, among the four typical traps (vacancy, GB, surface, dislocation) discussed in Section 2.1, only GB effects are focused on. Consequently, H atoms at the lattice sites and at GBs are only possible states of hydrogen in W in the present model, and the equations corresponding to Eqs. (1) and (2) are written as

$$D_{eff} = f_{H-lat}D_{H-lat} + f_{H-GB}D_{H-GB}, \tag{7}$$

$$f_{H-lat} + f_{H-GB} = 1. \tag{8}$$

A schematic drawing of the potential energy curve for H atom assumed in the present study is shown in Fig. 1. $E_{sol\text{-}lat}$ corresponds to the solution energy of hydrogen at lattice site of bcc-W, $E_{dif\text{-}lat}$ is the diffusion barrier of hydrogen at lattice sites, $E_{bind\text{-}GB}$ is the binding energy of hydrogen at GB, and $E_{dif\text{-}GB}$ is the diffusion barrier of hydrogen along GB.

Strictly speaking, $E_{bind\text{-}GB}$ and $E_{dif\text{-}GB}$ are dependent on GB type according to previous computational studies [14–18]. However, for simplicity, it is assumed in the present study that we can define effective values for these quantities, and then $E_{bind\text{-}GB}$ and $E_{dif\text{-}GB}$ correspond to such effective values. In addition, these effective values are assumed to be independent of temperature.

Furthermore, in the present study, only equilibrium conditions are considered for determination of $f_{H\text{-}lat}$ and $f_{H\text{-}GB}$ in Eq. (8). This setting is mostly for simplicity, but can be also justified because the purpose of the present study is to clarify how GB effects appear in the effective solubility, diffusivity and permeability observed in experiments. In experiments, these quantities are usually determined in (nearly) equilibrium states or in steady states, in which the local hydrogen distribution is expected to be close to that of the equilibrium state.

2.3. Derivation of thermodynamic model

With the research scope described in Section 2.2, what we need to do is to determine $f_{H\text{-}lat}$ and $f_{H\text{-}GB}$ in Eq. (8), and then to calculate the effective diffusivity, solubility and permeability based on the concept described in Section 2.1. In order to complete the task to determine $f_{H\text{-}lat}$ and $f_{H\text{-}GB}$, a thermodynamic model is established in this section based on the equilibrium theory.

First of all, model parameters are defined. The total number of H atoms in a poly-crystalline W specimen is defined as N_H, the number of lattice sites for hydrogen (interstitial tetrahedral sites, specifically) as N_L, and the number of GB sites for hydrogen as N_{GB}. With a variable x, which represents the fraction of H atoms trapped by GB sites and thus is identical to $f_{H\text{-}GB}$, the numbers of H atoms trapped at GBs and located in the lattice sites are expressed as xN_H and $(1-x)N_H$, respectively. The binding energy of H atoms at GBs is defined as $E_{bind\text{-}GB}$ as sketched in Fig. 1. For simplicity, $E_{bind\text{-}GB}$ is assumed to be independent of xN_H. This assumption is reasonably accurate in most relevant conditions, as will be explained later in this section.

Subsequently, the configurational entropy (S_{config}) of H atoms in this system is expressed as

$$S_{config} = k_B ln\left(W_{H-lat} \times W_{H-GB}\right), \tag{9}$$

where k_B is the Boltzmann constant, $W_{H\text{-}lat}$ is the number of configurational combinations for H atoms located over the lattice sites, and $W_{H\text{-}GB}$ is that for H atoms trapped over GB sites. $W_{H\text{-}lat}$ and $W_{H\text{-}GB}$ are functions of x and are expressed as

$$\ln\left(W_{H-lat}\right) = ln\left({}_{N_L}C_{(1-x)N_H}\right) \sim N_L \ln N_L - \left((1-x)N_H\right) \ln\left((1-x)N_H\right) - \left(N_L - (1-x)N_H\right) \ln\left(N_L - (1-x)N_H\right), \tag{10}$$

$$\ln\left(W_{H-GB}\right) = ln\left({}_{N_{GB}}C_{xN_H}\right) \sim N_{GB} \ln N_{GB} - (xN_H) \ln(xN_H) - (N_{GB} - xN_H) \ln(N_{GB} - xN_H), \tag{11}$$

where Starling's approximation, $\ln(N!) \sim N \ln N - N$, is applied.

Then, the free energy, specifically Helmholtz energy A, of the system is obtained as

$$A = -(xN_H)E_{bind-GB} - TS_{config}. \tag{12}$$

Note that the binding energy in the present study is defined to be positive if hydrogen is attracted by trap, so the minus sign is added to the energy term in Eq. (12). It is assumed that the vibrational entropy and the electronic entropy are not largely different between the lattice sites and GB sites so that terms related to these entropies disappear in Eq. (12). If we can further assume that the binding energy is nearly equal to the binding enthalpy, which is usually accurate in condensed phases unless the pressure is extremely high, the Helmholtz energy in Eq. (12) can be replaced with the Gibbs energy.

In Eq. (12), S_{config} is a function of x, and then A is so. Therefore, the minimum free energy, which is the condition of equilibrium state, is achieved when the partial derivative of A with respect to x is 0, namely

$$\frac{\partial A}{\partial x} = N_H \left\{ -E_{bind-GB} - k_B T \ln \left\{ \frac{(1-x)(N_{GB} - xN_H)}{x(N_L - (1-x)N_H)} \right\} \right\} = 0. \quad (13)$$

This equation is converted to the following quadratic equation regarding x:

$$x^2 + ax + b = 0, \quad (14)$$

with

$$a = \frac{-N_L \exp\left(-E_{bind-GB}/k_B T\right) - N_{GB}}{N_H \left(1 - \exp\left(-E_{bind-GB}/k_B T\right)\right)} - 1, \quad (15)$$

$$b = \frac{N_{GB}}{N_H \left(1 - \exp\left(-E_{bind-GB}/k_B T\right)\right)}. \quad (16)$$

One of two roots of the quadratic equation that holds a value between 0 and 1 is what we look for.

DFT calculation showed that $E_{bind\text{-}GB}$ depends on the occupation of GB sites (xN_H/N_{GB}) [14,15]. If the dependence is taken into account, the forms of Eq. (13) and then Eq. (14) are altered. However, it is reasonable to assume that $E_{bind\text{-}GB}$ is constant and independent of xN_H/N_{GB}, if $xN_H/N_{GB} << 1$ is achieved. This is because no significant interaction between two H atoms trapped at GB is induced in such a condition where H atoms do not densely occupy GB sites. Indeed, $xN_H/N_{GB} << 1$ is satisfied in most conditions examined in the present paper, as will be shown in Section 3.7.

In Appendix A, a method to determine x with $E_{bind\text{-}GB}$ depending on xN_H/N_{GB} will be also presented.

2.4. Determination of model parameters

2.4.1. N_L and N_{GB}

Among the four parameters (N_L, N_{GB}, $E_{bind\text{-}GB}$, N_H,) involved in Eq. (14), we can determine N_L and N_{GB} by assuming the shape of grains. In the present study, the shape is assumed to be cubic, and a poly-crystalline W specimen composed of cubic grains of the same size is considered. Consequently, the following relations are achieved:

$$N_{cell} = l_{grain}/l_{lat}, \quad (17)$$

$$N_L = \alpha N_{cell}^3, \quad (18)$$

$$N_{GB} = 3\beta N_{cell}^2, \quad (19)$$

$$N_M = \gamma N_{cell}^3, \quad (20)$$

where N_{cell} is the number of conventional bcc unit cells aligning along ⟨100⟩ direction of the cubic grain, l_{grain} [μm] is the size of the cubic grain, l_{lat} [μm] is the lattice constant of bcc-W (0.316×10^{-3} μm), α is the number of tetrahedral interstitial sites in each conventional unit cell of bcc lattice, β is the number of GB sites on each {100} plane of the unit cell, N_M is the number of W atoms in each grain, and γ is the number of W atoms in the unit cell. Since each cubic grain holds 6 GB planes and each plane is shared by 2 neighboring grains, $\beta N^2{}_{cell}$ should be multiplied by 3 as done in Eq. (19). For bcc lattice, α and γ are unambiguously set to be 12 and 2, respectively.

2.4.2. β and $E_{bind\text{-}GB}$

The value of β holds some uncertainty. One DFT study on Σ5 tilt GB showed that the GB can capture up to 2 H atoms per unit GB plane [14], while the other on Σ3 tilt GB up to 6 H atoms [15]. In both cases, the addition of H atom generally reduces the binding energy due to repulsive interaction between trapped H atoms. Specifically, the binding energies ($E_{bind\text{-}GB}$) to Σ5 tilt GB for the 1st and 2nd H atoms are around 1.1 eV and 1.0 eV, respectively [14], while the binding energies to Σ3 tilt GB for the 1st, 2nd, 3rd, and 4th H atoms are around 1.2 eV, 1.0 eV, 0.8 eV and 0.3 eV, respectively [15].

In the present study, β is set to be 2 and $E_{bind\text{-}GB}$ to be 1.0 eV based on the DFT calculation results mentioned above. Since the binding energy to GB is assumed to be a constant, a large value like 4 is inappropriate for β. 1.0 eV for $E_{bind\text{-}GB}$ is also reasonably consistent with the binding energy to W(110)/W(112) interface obtained by DFT calculation [16]. In order to confirm the appropriateness of $E_{bind\text{-}GB}$ = 1.0 eV, results of sensitivity analyses on $E_{bind\text{-}GB}$ are also shown in Chapter 3 with varying $E_{bind\text{-}GB}$ from 0.5 eV to 1.4 eV.

2.4.3. N_H

N_H may be considered to be an arbitrary parameter if we are interested in hydrogen distribution in the system with a given hydrogen concentration. On the other hand, if we are interested in a comparison with experiments, for example those evaluating the permeability of hydrogen loaded into the specimen through H_2 gas absorption, we should determine N_H equilibrated with the H_2 gas. This is achieved based on the Sieverts' law as follows:

$$\frac{(1-x)N_H}{N_M} = \frac{N_{Av}}{\rho_M} \times \sqrt{p_{H2}} \times 2S_{H-lat}, \quad (21)$$

where N_{Av} is the Avogadro constant, ρ_M [m^{-3}] is the number density of W atoms, p_{H2} [Pa] is the partial pressure of the H_2 gas, and $S_{H\text{-}lat}$ [mol m^{-3} $Pa^{-0.5}$] is the hydrogen solubility in the lattice sites. $(1-x)N_H/N_M$ is the concentration of hydrogen in the lattice sites in H/W unit. The factor 2 is for conversion from the number of H_2 molecules to the number of H atoms in order to obtain the concentration of H atoms in the lattice. ρ_M is expressed with γ used in Eq. (20) as

$$\rho_M = \gamma / \left(l_{lat} \times 10^{-6}\right)^3. \quad (22)$$

Sieverts' law is established by equating the chemical potential of H atom in H_2 gas with that of H atom solute in the lattice [42], with conditions that (i) the temperature is not very low and the pressure is not very high so that the H_2 gas behaves like ideal gas, and that (ii) the concentration of the solute H atom is not high so that there is no significant distortion in the lattice structure, no significant interaction between solute H atoms, and no formation of hydrides. Since the chemical potential of H atom solute in the lattice is not changed by existence of GBs unless the grain size is extremely small, the equilibrium concentration of hydrogen in the lattice sites should not be affected by GBs. Thus, Sieverts' law appropriately provides the equilibrium concentration of H atoms at the lattice sites even for poly-crystalline materials.

Eq. (21) is a condition that N_H and x need to satisfy in addition to Eq. (14). In practice, after determining N_H by using Eq. (21) with an initial guess of x, Eq. (14) is solved with determined N_H to update x. Then, one decreases or increases x toward the direction that x become more consistent between Eqs. (14) and (21). This process is repeatedly continued until a required accuracy in the consistency is achieved. A set of N_H and x that simultaneously satisfy Eqs. (14) and (21) represent the distribution of hydrogen in poly-crystalline W equilibrated with H_2 gas of p_{H2} Pa. Note that a high precision is required for numerical calculation of x because the exponential terms in Eqs. (15) and (16) become very small especially at low temperatures like room temperature.

2.5. Formulation of effective solubility, diffusivity and permeability

2.5.1. Effective diffusivity

With the method described in Section 2.4, N_H and x are determined with given grain size (l_{grain}), temperature (T) and partial pressure of H_2 gas (p_{H2}). l_{grain}, T and p_{H2} can be set based on experimental conditions. Then, with $f_{H\text{-}lat} = (1-x)$ and $f_{H\text{-}GB} = x$, the effective diffusivity is expressed by Eq. (7) if $D_{H\text{-}lat}$ and $D_{H\text{-}GB}$ are known. $D_{H\text{-}lat}$ is equivalent with hydrogen diffusivity in a single-crystal bcc-W where trap effects of lattice defects are negligible. The equation suggested by Heinola et al. [35], which was fit only to high-temperature data of Frauenfelder's experiment [34] in order to avoid trap effects at low temperatures [12], is employed for it:

$$D_{H-lat}[\mathrm{m^2 s^{-1}}] = 1.58 \times 10^{-7} \times \exp\left(-0.25eV/k_BT\right). \quad (23)$$

The value of D_{H-GB} is uncertain at present. Regarding its pre-exponential factor, for simplicity, it is assumed to be equal to the pre-exponential factor of D_{H-lat}. This assumption would be justified as follows. In general, the pre-exponential factor of diffusion coefficients (D_0) is expressed by the attempt frequency of atomic jump to a neighboring site ($\nu_{attempt}$), the distance of each jump (d_{jump}), the number of equivalent paths for the jump (n_{path}) and the correlation factor in consecutive jumps (f_{corr}) as

$$D_0 = n_{path} f_{corr} d_{jump}^2 \nu_{attempt}/6. \quad (24)$$

f_{corr} is basically 1 for impurity diffusion like hydrogen diffusion in W. Then, because the other three parameters (n_{path}, d_{jump}, $\nu_{attempt}$) are expected to be not largely different between jumps of H atoms in the lattice and along GBs, probably the difference is within an order of magnitude, it is reasonable to use the same pre-exponential factor for $D_{H\text{-}GB}$ with $D_{H\text{-}lat}$. Consequently, $D_{H\text{-}GB}$ is expressed as

$$D_{H-GB}[\mathrm{m^2 s^{-1}}] = 1.58 \times 10^{-7} \times \exp\left(-E_{dif-GB}/k_BT\right), \quad (25)$$

where $E_{dif\text{-}GB}$ is the diffusion barrier for H atom along GB.

In a previous MD study [18] with Li's potential model [27], the activation energy of effective hydrogen diffusivity was obtained to be around 0.7 eV in poly-crystalline W composed of 5 nm grains over 1200–2000 K with 0.1–10% H/W ratios [18]. Although the temperature is high, since a high density of GBs are brought by 5 nm grains, the main diffusion mechanism for hydrogen should be the diffusion along GBs in this system and then 0.7 eV should correspond to $E_{dif\text{-}GB}$. With this potential model, $E_{dif\text{-}lat}$ was obtained in a single-crystal system to be around 0.2 eV [18], which is comparable with the value used in the present study (0.25 eV in Eq. (23)). Thus, one possible choice for $E_{dif\text{-}GB}$ is 0.7 eV.

Another MD study [19] with the same Li's potential model showed that hydrogen diffusivity in a GB region is smaller than that in the bulk region at 600 K, while the former becomes larger than the latter at 900 K and 1200 K. This result indicates a larger diffusion barrier and a larger pre-exponential factor at the GB region than those in the bulk. However, this Li's potential model is prone to overestimate the binding energy to GB: for Σ5 tilt GB, Li's potential model calculates the binding energy to be around 2.5 eV [19], while DFT around 1.1 eV [14]. Therefore, the value 0.7 eV for $E_{dif\text{-}GB}$ is not free of error, probably overestimated.

In DFT studies on high-symmetry GBs like Σ5 tilt GB [14] and W(110)/W(112) interface [16], small diffusion barriers along GB were found, like $E_{dif\text{-}GB} < 0.2$ eV. This value is even smaller than $E_{dif\text{-}lat}$. Although this kind of small barrier was also found by classical MD with Juslin's potential model, a thorough investigation over various possible GBs showed that the whole spectrum of barriers broadly range from 0 eV to 3 eV [17]. It is reasonable to think that a similar wide spectrum in the barriers is obtained with Li's potential model as well as by DFT calculation, although not confirmed yet. As the effective barrier over various GBs became around 0.7 eV with Li's potential model [18], the effective value for $E_{dif\text{-}GB}$ in practical materials is likely to be larger than $E_{dif\text{-}lat}$.

Consequently, $E_{dif\text{-}GB}$ is set to be 0.4 eV in the present study. This value is consistent with the discussion above. In addition, calculation results with $E_{dif\text{-}GB} = 0.4$ eV nicely reproduce experimental data of hydrogen diffusivity at low temperatures (300–700 K), as will be presented in Section 3.2. Nevertheless, as the uncertainty in $E_{dif\text{-}GB}$ is large, results of sensitivity analyses on $E_{dif\text{-}GB}$ are also presented in Chapter 3 with varying $E_{dif\text{-}GB}$ from 0.2 eV to 1 eV.

2.5.2. Effective solubility

The effective solubility is calculated as follows in analogy with Eq. (21):

$$\frac{N_H}{N_M} = \frac{N_{Av}}{\rho_M} \times \sqrt{p_{H2}} \times 2S_{eff}. \quad (26)$$

In order to determine N_H, we need to fix the solubility of hydrogen in the lattice ($S_{H\text{-}lat}$), which should be close to the solubility determined by experiment with a well-annealed specimen at high temperatures.

In experiments, hydrogen solubility is often determined from the relation among the solubility, diffusivity and permeability, like $P = SD$. And it is known that permeability data are less scattered and thus more reliable than solubility and diffusivity data in experiments, especially at high temperatures. In the present study, the hydrogen diffusivity in the lattice is described with Eq. (23), which was obtained [35] by re-evaluating the diffusivity of Frauenfelder's experiment [34]. Therefore, in order to make the permeability calculated by $P = SD$ consistent with that measured in the same Frauenfelder's experiment, the solubility of Frauenfelder's experiment needs to be also re-evaluated. This re-evaluation gives the following expression for hydrogen solubility in the lattice ($S_{H\text{-}lat}$ [$\mathrm{mol\,m^{-3}\,Pa^{-0.5}}$]):

$$S_{H-lat} = 3.8 \times \exp\left(-E_{sol-lat}/k_BT\right), \quad (27)$$

where $E_{sol\text{-}lat}$ is 1.18 eV. As designed, the permeability ($P_{H\text{-}lat}$ [$\mathrm{mol\,m^{-1}\,s^{-1}\,Pa^{-0.5}}$]) calculated as the product of $S_{H\text{-}lat}$ and $D_{H\text{-}lat}$, which are respectively expressed by Eqs. (27) and (23), becomes equal to the permeability of Frauenfelder's experiment [34], namely

$$P_{H-lat} = 6.0 \times 10^{-7} \times \exp\left(-E_{perm-lat}/k_BT\right), \quad (28)$$

where $E_{perm\text{-}lat}$ is 1.43 eV.

Regarding the units of solubility and permeability, in accordance with the convention, 'mol' is of H_2 molecule in the lattice of W although the chemical state of H in the lattice is H atom, and 'Pa' is of H_2 molecules in the gas phase. These units for solubility and permeability are used throughout the present paper.

2.5.3. Effective permeability

The effective permeability is simply determined as

$$P_{eff} = S_{eff} D_{eff}, \quad (29)$$

assuming that surface processes do not control the rate of hydrogen permeation. As described in Section 2.1, this assumption seems to be often valid in W.

2.6. Summary of the model

The model structure is summarized in Fig. 2 and the model parameters are summarized in Table 1. Since relatively large uncertainties are expected in $E_{bind\text{-}GB}$ and $E_{dif\text{-}GB}$, and l_{grain} is largely dependent on experiments, sensitivity analyses were preformed on these three parameters by varying them in the following ranges: 0.5–1.4 eV for $E_{bind\text{-}GB}$, 0.2–1 eV for $E_{dif\text{-}GB}$, and 0.01–100 μm for

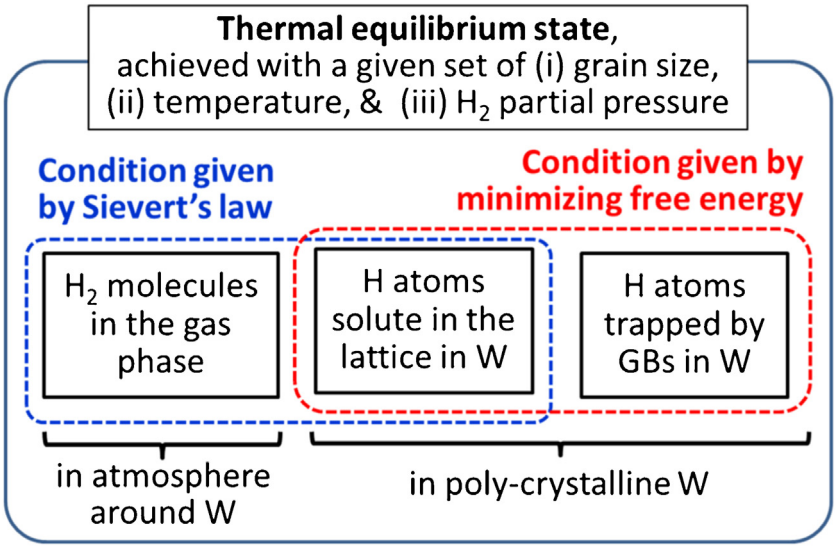

Fig. 2. Summary of the structure of the thermodynamic model.

Table 1
Summary of model parameters. For l_{grain}, $E_{bind-GB}$ and E_{dif-GB}, the values in parentheses are of the reference values.

Parameter	Definition	Value
l_{grain}	Grain size	0.01–100 μm (10 μm)
l_{lat}	Lattice constant of bcc-W	0.316×10^{-3} μm
α	Number of interstitial tetrahedral sites in each unit cell	12
β	Number of hydrogen trapping sites per unit GB plane	2
γ	Number of W atoms in each unit cell	2
p_{H2}	Partial pressure of H_2 in the gas phase	1×10^5 Pa
$E_{sol-lat}$	Solution energy of hydrogen in the lattice	1.18 eV
$E_{bind-GB}$	Effective binding energy of hydrogen to GBs	0.5–1.4 eV (1.0 eV)
$E_{dif-lat}$	Diffusion barrier of hydrogen in the lattice	0.25 eV
E_{dif-GB}	Effective diffusion barrier of hydrogen along GBs	0.2–1.0 eV (0.4 eV)

l_{grain}. Hereafter, $E_{bind-GB} = 1.0$ eV, $E_{dif-GB} = 0.4$ eV and $l_{grain} = 10$ μm are called reference values.

As for H_2 partial pressure (p_{H2}), it is set to be 1×10^5 Pa unless specified. Note that the effective solubility, diffusivity and permeability are hardly dependent on p_{H2} unless the partial pressure is extremely high. The dependences on p_{H2} will be explained in Section 3.6.

2.7. Experimental data for comparison

D_{eff} and P_{eff} calculated by the constructed thermodynamic model are compared with available experimental data in Chapter 3. Since the available data on S_{eff} is limited, such comparison is not made for it.

The experimental data used in the comparisons are labelled with the author's name and the year of publication as follows:

- Diffusivity: Frauenfelder-1969 [34]; Zakharov-1975 [43]; Esteban-2001 [44]; Nakamura-2003 [41]; Otsuka-2009 [45]; Gasparyan-2009 [46]; Heinola-2010 [35]; Ikeda-PDP-2011 [47]; Ikeda-GDP-2011 [48].
- Permeability: Aitken-1967 [49]; Frauenfelder-1968 [39]; Frauenfelder-1969 [34]; Zakharov-1975 [43]; Benamati-2000 [40]; Esteban-2001 [44].

Pre-exponential factors (D_0 [$m^2\ s^{-1}$] and P_0 [$mol\ m^{-1}\ s^{-1}\ Pa^{-0.5}$]) and activation energies (E_D and E_P [$kJ\ mol^{-1}$]) for Arrhenius equations of hydrogen diffusivity and permeability in these experiments are summarized in Tables 2 and 3. Table 2 shows values obtained by gas permeation experiment (gas-driven permeation, GDP), and Table 3 shows values obtained by other experimental methods including gas desorption experiment, ion-driven permeation (IDP) experiment, plasma-driven permeation (PDP) experiment, etc. T was used as hydrogen in Nakamura-2003, Otsuka-2009, Ikeda-PDP-2011 and Ikeda-GDP-2011, D was used in Gasparyan-2009, and H was used in the other experiments.

In Table 2 for gas permeation experiment, the values of Aitken-1967 are taken from a literature compiled by Steward [50] because the original paper could not be obtained. In Frauenfelder-1968, Benamati-2000 and Ikeda-GDP-2011, poly-crystalline W specimens were utilized. The sample specification of Aitken-1967 is not provided in the complied literature [50].

In Zakharov-1975, experiments with both single-crystalline and poly-crystalline W specimens were performed, which showed that differences between single-crystals and poly-crystals in the diffusivity and the permeability were small in comparison with experimental errors [43]. Due to the small differences, Arrhenius equations for the diffusivity and the permeability were derived from results of both types of crystals [43]. In the present study, the temperature range of the diffusivity is restricted to 920–1050 K where experimental data were presented in a figure in Ref. [43].

In Ikeda-GDP-2011, H_2 and T_2 gas mixture (T/H ratio of 1.25×10^{-4}) was used.

In Table 3, all experiments were performed with poly-crystalline W specimens. The results of Frauenfelder-1969 and Esteban-2001 were derived from degas experiment of thermally absorbed H_2 [34,44]. In degas experiment, effective solubility and effective diffusivity are determined and then effective permeability

Table 2
Summary of diffusivity and permeability determined by gas permeation experiment.

Reference	D_0 ($m^2\ s^{-1}$)	E_D ($kJ\ mol^{-1}$)	P_0 ($mol\ m^{-1}\ s^{-1}\ Pa^{-0.5}$)	E_P ($kJ\ mol^{-1}$)	Temp. (K)	Pressure (kPa)
Aitken-1967			7.77×10^{-7}	141	1600–2900	$10–10^2$
Frauenfelder-1968			7.6×10^{-7}	132	1050–2400	10^{-7}–27
Zakharov-1975			5.4×10^{-8}	106	673–1473	0.13–27
	2.4×10^{-4}	94.8			920–1050	0.13–1.3
Benamati-2000			3.0×10^{-10}	71.9	720–850	$10–10^2$
Ikeda-GDP-2011	3.4×10^{-9}	37.7			298–353	3

Table 3
Summary of diffusivity and permeability determined by other experimental techniques.

Reference	D_0 ($m^2\ s^{-1}$)	E_D ($kJ\ mol^{-1}$)	P_0 ($mol\ m^{-1}\ s^{-1}\ Pa^{-0.5}$)	E_P ($kJ\ mol^{-1}$)	Temp. (K)
Frauenfelder-1969	4.1×10^{-7}	37.7	6.0×10^{-7}	138	1100–2400
Esteban-2001	5.68×10^{-10}	9.3	1.65×10^{-11}	36.2	823–1073
Nakamura-2003	3.3×10^{-9}	55.7			590–670
Gasparyan-2009	4.9×10^{-2}	193			823–923
Otsuka-2009	3×10^{-7}	37.6			473–673
Heinola-2010	1.58×10^{-7}	24.1			
Ikeda-PDP-2011	1.0×10^{-8}	31.4			308–343

can be calculated with Eq. (29) if surface processes are not rate-determining steps. Strictly speaking, the diffusivity of Esteban-2001 is not an effective diffusivity because a trap effect was removed using a theoretical model [44]. However, the trap effect was not significant above 823 K. Therefore, in the present study, the temperature range of Esteban-2001 is restricted to 823–1073 K where the diffusivity given in Table 3 nicely reproduce the effective diffusivity presented in Ref. [44].

In Otsuka-2009, the diffusivity was determined by analyzing time evolution of tritium depth profile using tritium imaging plate technique [45]. Tritium was initially loaded into samples by DC glow discharge of H_2 and T_2 gas mixture (T/H ratio of 10^{-4}). In Ikeda-PDP-2011, the diffusivity was determined in permeation experiments of T. DC glow discharge was utilized to load T into specimens.

In Nakamra-2003 and Gasparyan-2009, the diffusivity was determined in permeation experiments of hydrogen loaded in W specimens by ion irradiation. In Nakamura-2003, 1 keV T^+ ion was irradiated with a flux of $9 \times 10^{18}\ T\ m^{-2}\ s^{-1}$. In Gasparyan-2009, 600 eV D_3^+ ion was irradiated with a flux of 10^{17}–$10^{18}\ D\ m^{-2}\ s^{-1}$.

In Heinola-2010, the diffusivity was obtained by refitting only high-temperature data (1500–2500 K) of Frauenfelder-1969 [35], excluding two data points of lower temperatures in order to avoid trap effects at low temperatures [12].

In summary, except for Aitken-1967, the permeability and diffusivity data listed in Table 2 and 3 are effective values of poly-crystal specimens (or nearly equivalent with effective values), and thus should include GB effects and are appropriate to be compared with the present model. Whether the specimen was single-crystal or poly-crystalline is not clear in Aitken-1967. However, the obtained permeability in Aitken-1967 should be hardly affected by GBs even if the sample was poly-crystalline, because the experimental temperature was very high (1600–2900 K). In such a high temperature, GB effects become negligibly small, which is to be confirmed in Chapter 3 in the present study.

With regard to the grain sizes of W specimens in the experiments, they were a few μm in Gasparyan-2009, and were a few ten μm in Esteban-2001. Note that the grain sizes in Esteban-2001 is an estimation from a micrographic picture presented in Ref. [44]. These sizes are comparable with grain sizes assumed in the present study. In Frauenfelder-1969 and Zakharov-1975, micrographic pictures of specimens are also presented, although the scale is not clear. In the other studies, grain sizes are not specifically described.

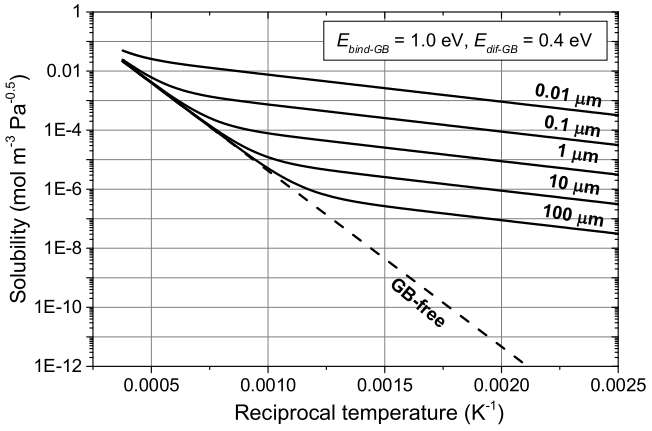

Fig. 3. Comparison of effective hydrogen solubility (S_{eff}) calculated with various grain sizes (l_{grain}).

3. Results

3.1. GB effects in hydrogen solubility

Fig. 3 compares effective hydrogen solubility (S_{eff}) calculated with various grain sizes (l_{grain}). $E_{bind\text{-}GB}$ and $E_{dif\text{-}GB}$ were fixed to be the reference values, 1.0 eV and 0.4 eV, respectively. Since the area of GBs increases as the grain size decreases, larger influence of GBs is observed in a smaller grain. The solubility in GB-free system, which is a perfect single-crystal specimen of the infinite size of grain, is expressed by Eq. (23) and then is presented by dash line and labelled with "GB-free" in Fig. 3 and other figures.

The slope of the temperature dependence of the solubility in the GB-free system corresponds to 1.18 eV, which is equal to $E_{sol\text{-}lat}$. The slopes in poly-crystalline systems also converge to 1.18 eV at high temperatures. This is because the entropy effect causes a higher fraction of H atoms to stay in the lattice sites at a higher temperature, and then H atoms in the lattice sites becomes the dominant state at sufficiently high temperatures. This trend is clearly seen in temperature dependence of $f_{H\text{-}lat}$ presented in Fig. 4. On the other hand, at low temperatures, the slopes converge to $E_{sol\text{-}lat} - E_{bind\text{-}GB}$, which is the energy difference between H atom trapped by GB and H atom composing H_2 molecule in the gas phase. For example, the slope in l_{grain} = 10 μm case is around 0.18 eV below 600 K, as $E_{sol\text{-}lat} - E_{bind\text{-}GB}$ = 1.18 eV − 1.0 eV = 0.18 eV. This low temperature behavior indicates that the dominant hydrogen state at low tem-

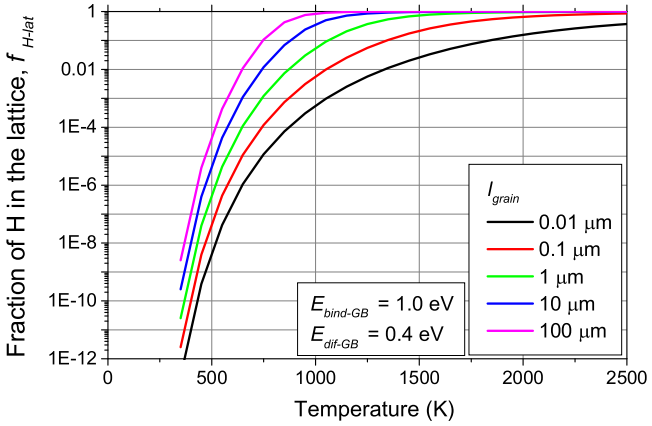

Fig. 4. Temperature dependence of the fraction of H atoms located in the lattice sites ($f_{H\text{-}lat}$) with various grain sizes (l_{grain}).

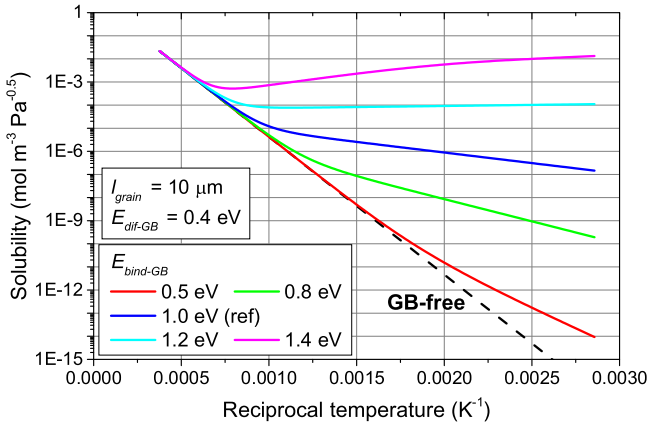

Fig. 5. Influence of the binding energy to GBs ($E_{bind\text{-}GB}$) on effective hydrogen solubility (S_{eff}).

peratures is H atoms trapped by GBs in poly-crystalline W, which is also confirmed in Fig. 4.

Fig. 5 shows the influence of $E_{bind\text{-}GB}$ on S_{eff}. Even if a small binding energy like 0.5 eV is applied, GBs induce a non-negligible increase in S_{eff}. This is because GB sites are usually abundant in practical materials. Specifically, with cubic grains, the ratio of GB sites to the lattice sites for H atoms is expressed as

$$\frac{N_{GB}}{N_L} = \frac{\alpha N^3}{3\beta N^2} = \frac{\alpha l_{grain}}{3\beta l_{lat}}. \quad (30)$$

For example with l_{grain} = 10 μm, the ratio becomes 6.3×10^{-5}, which is much larger than the concentration of other traps such as vacancy in most equilibrium conditions except for those at very high temperatures. Due to the abundancy, the effect of GBs is enormous at low temperatures and still remains significant up to a high temperature like 1000 K even if a small $E_{bind\text{-}GB}$ value is assumed.

Since hydrogen solution energy is 1.18 eV, if $E_{bind\text{-}GB}$ is larger than 1.18 eV like 1.2 eV and 1.4 eV in Fig. 5, namely if $E_{bind\text{-}GB} > E_{sol\text{-}lat}$ is achieved, the potential energy of H atom trapped by GB becomes smaller than that of H atom composing H_2 molecule in the gas phase. In such cases, more H atoms occupy GB sites at lower temperatures, and some of them move to the gas phase by temperature increase due to the entropy effect. Thus, the effective solubility decreases as the temperature increases, as shown in the results of $E_{bind\text{-}GB}$ = 1.2 eV and $E_{bind\text{-}GB}$ = 1.4 eV cases in Fig. 5.

A result on the influence of $E_{dif\text{-}GB}$ on S_{eff} is omitted because S_{eff} is independent of $E_{dif\text{-}GB}$.

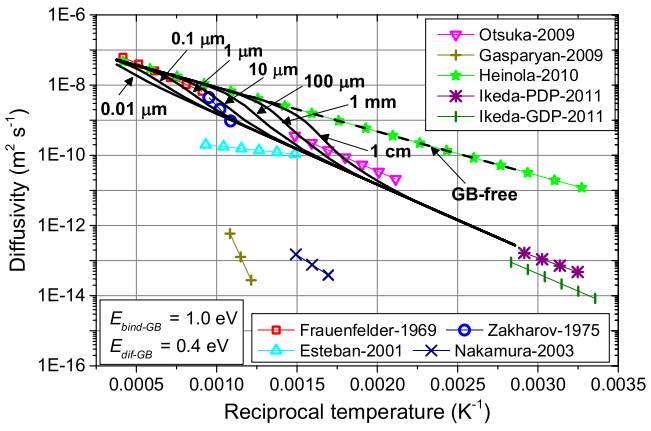

Fig. 6. Comparison between effective hydrogen diffusivity (D_{eff}) calculated with various grain sizes (l_{grain}) and experimental results. Marks on lines of experimental results are used for visualization purpose and are not measured data points of experiments.

3.2. GB effects in hydrogen diffusivity

Fig. 6 compares effective hydrogen diffusivity (D_{eff}) calculated with various grain sizes (l_{grain}). $E_{bind\text{-}GB}$ and $E_{dif\text{-}GB}$ were fixed to be the reference values. The data of the GB-free system, given with dash line and labelled "GB-free", is expressed by Eq. (23), which corresponds to the diffusivity in singe-crystal W of the infinite size. As a general trend in Fig. 6, effects of GBs are more pronounced for smaller grain sizes because more GB sites are involved in the system.

In comparison with trap effects by vacancy, the reduction of effective diffusivity caused by GBs is much smaller than that by vacancy [12]. This is because H trapped at GBs can still diffuse in the system along GBs. In a general trend, D_{eff} converges to $D_{H\text{-}lat}$ at high temperatures unless the grain size is very small like 0.01–0.1 μm, while it converges to $D_{H\text{-}GB}$ at low temperatures. This trend is due to the entropy effect as explained in Section 3.1 and as seen in Fig. 4.

The model with $E_{dif\text{-}GB}$ = 0.4 eV nicely reproduces the effective diffusivity of some experiments, specifically Otsuka-2009, Ikeda-PDP-2011 and Ikeda-GDP-2011. In these experiments, the diffusivity was determined at low temperatures (around 300–700 K) [45,47,48], where the dominant diffusion mechanism is the diffusion along GBs as shown in Fig. 6. Therefore, it is more appropriate to assign the diffusivity of Otsuka-2009, Ikeda-PDP-2011 and Ikeda-GDP-2011 to the diffusivity along GBs ($D_{H\text{-}GB}$), not to that in the lattice ($D_{H\text{-}lat}$).

Even with 1 mm or 1 cm grain, D_{eff} is largely affected by GBs below 600 K and becomes almost equal to $D_{H\text{-}GB}$ below 500 K. The grain size of 1–10 mm is comparable with that of commercially available single-crystals. DFT calculation on a W surface indicated that the migration barrier for hydrogen diffusion on (100) surface is 0.43 eV [36], which is comparable with the reference value of $E_{dif\text{-}GB}$ (0.4 eV), and the binding energy to the same surface is 1.86 eV [36], which is larger than the reference value of $E_{bind\text{-}GB}$ (1.0 eV). Therefore, even if a single-crystal is used in experiments, hydrogen diffusion on the surface would largely contribute to D_{eff} unless hydrogen diffusion through the surfaces of side planes is avoided. It seems that determining $D_{H\text{-}lat}$ in experiments is technically difficult at low temperatures like below 600 K, which is basically due to the large positive solution energy for hydrogen in W lattice.

Fig. 7 shows the influence of $E_{dif\text{-}GB}$ on D_{eff}. If $E_{dif\text{-}GB}$ is set to be smaller than $E_{dif\text{-}lat}$, like 0.20 eV, D_{eff} becomes larger than $D_{H\text{-}lat}$ as shown in Fig. 7. On the other hand, if a large value like 0.6 eV is set, GBs act like a deep trap because H atoms trapped by GBs

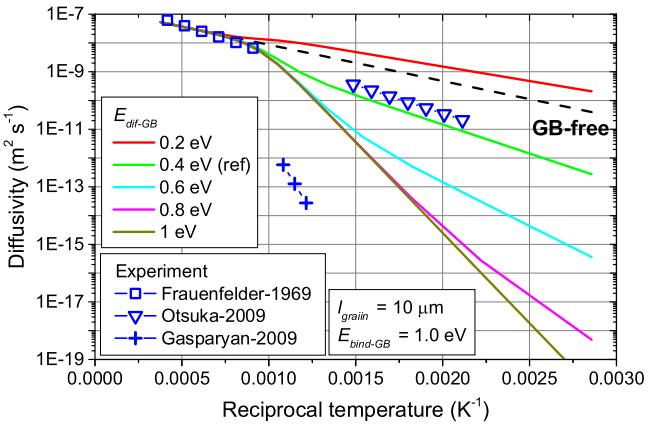

Fig. 7. Influence of the diffusion barrier along GBs ($E_{dif\text{-}GB}$) on effective hydrogen diffusivity (D_{eff}).

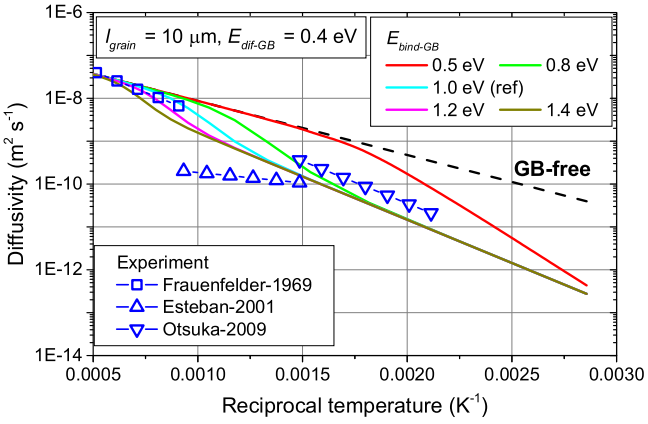

Fig. 8. Influence of the binding energy to GBs ($E_{bind\text{-}GB}$) on effective hydrogen diffusivity (D_{eff}).

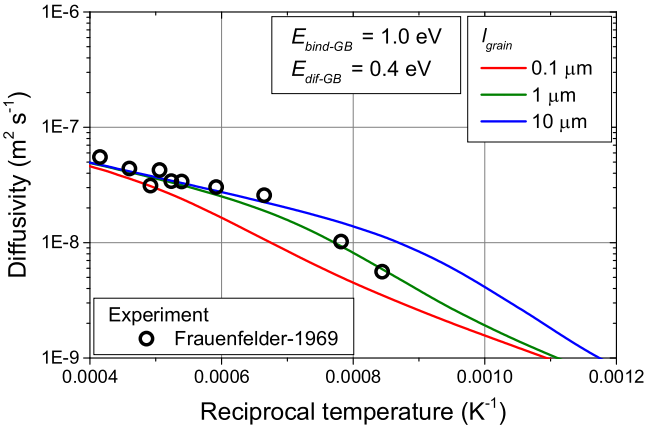

Fig. 9. Detailed comparison on effective hydrogen diffusivity between model calculation results and experimental data points of Frauenfelder-1969.

hardly move with a large $E_{dif\text{-}GB}$. In both cases, the slope and the absolute values of D_{eff} disagree with the experimental results at low temperatures (300–700 K). Thus, 0.4 eV seems to be the most likely value for $E_{dif\text{-}GB}$. The uncertainty in it would be around ±0.1 eV, at most ±0.2 eV.

Regarding the diffusivity of Zakharov-1975, Nakamura-2003 and Gasparyan-2009, it is more appropriate to relate these results with other deeper traps like vacancy than with GBs. Indeed, the authors of Nakamura-2003 and Gasparyan-2009 pointed out possible influence of traps in their results [41,46]. In addition, effects of vacancy-type trap can nicely explain the deviation of these data from Eq. (23), especially for Zakharov-1975 [10] and Gasparyan-2009 [12]. On the other hand, Esteban-2001 cannot be explained with the present model nor with the vacancy model [12]. In order to explain Estenban-2001, we may need to construct a more sophisticated model, for example, like a model to consider both GB effects and vacancy-type trap effects simultaneously, which is a subject for future study.

Fig. 8 shows the influence of $E_{bind\text{-}GB}$ on D_{eff}. Even with a relatively small binding energy, e.g. $E_{bind\text{-}GB}$ = 0.5 eV, significant GB effects are observed below 500 K. 0.8 eV would be around the lower limit for $E_{bind\text{-}GB}$ to reproduce Otsuka-2009, while 1.2 eV would be around the upper limit to reproduce Frauenfelder-1969.

3.3. Detailed comparison with frauenfelder-1969

The diffusivity of Frauenfelder-1969 [34] has been most widely utilized in previous studies as hydrogen diffusivity in the lattice of bcc-W, namely $D_{H\text{-}lat}$. It is expressed as

$$D_{Frauenfelder-1969}[\mathrm{m^2 s^{-1}}] = 4.1 \times 10^{-7} \times \exp\left(-0.39eV/k_BT\right). \quad (31)$$

Our previous study using KMC simulation confirmed that two low-temperature data points in Frauenfelder's experiment [34] could be affected by vacancy-type traps [12], as suggested by Heinola et al. [35]. One may think that the deviation of the low-temperature data points in the Frauenfelder's experiment may be also explained by GB effect. Fig. 9 shows detailed comparison between the measured data points of Fraunfelder-1969 and the calculation results obtained with l_{grain} = 0.1 μm, 1 μm or 10 μm. $E_{bind\text{-}GB}$ and $E_{dif\text{-}GB}$ are fixed to be the reference values. The result of l_{grain} = 1 μm reasonably reproduces the deviation of the two low-temperature data points.

In the Frauenfelder's paper [34], a photo of crystal grains is presented with no scale, and the grain size in the experiment is not specifically described in the main body. Therefore, it is difficult to deepen the discussion more. Nevertheless, the present result reconfirms that the two low-temperature data in the Frauenfelder's study [34] are significantly affected by lattice defects, such as vacancy or/and GBs or/and else. And it is also confirmed that experimental data obtained at high temperatures like T > 1500 K are hardly affected by GB and by vacancy [12] unless the grain size is very small and unless the vacancy concentration is very high, respectively. Therefore, as proposed by Heinola et al. [35], excluding the two low-temperature data is appropriate to obtain the diffusivity of hydrogen in the lattice of W ($D_{H\text{-}lat}$). Accordingly, Eq. (23) should be a more appropriate equation for $D_{H\text{-}lat}$, not Eq. (31) which was derived in the Frauenfelder's paper [34].

3.4. GB effects in hydrogen permeability

Fig. 10 compares effective hydrogen permeability (P_{eff}) calculated with various grain sizes (l_{grain}). $E_{bind\text{-}GB}$ and $E_{dif\text{-}GB}$ were fixed to be the reference values. The data of the GB-free system, given with dash line and labelled "GB-free", is expressed by Eq. (28), which corresponds to the result in singe-crystal W of the infinite size. Roughly speaking, the GB effect is visible below around 1000 K for 10 μm grain and below around 1200 K for 1 μm grain. This result agrees with a trend in experimental data: experimental results at temperatures below around 1000–1200 K show some disagreement with each other, while those at higher temperatures show good agreement.

If a fine-grain material is used as a specimen, e.g. l_{grain} = 0.1 μm, the temperature where the GB effect becomes visible shifts to the higher temperature side and becomes unclear. In such a case, the

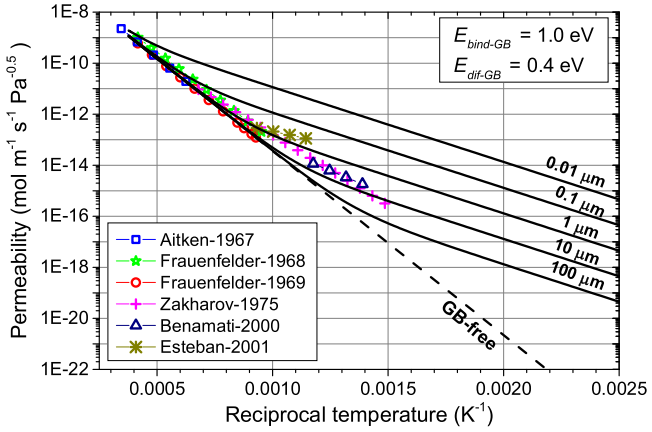

Fig. 10. Comparison between effective hydrogen permeability (P_{eff}) calculated with various grain sizes (l_{grain}) and experimental results. Marks on lines of experimental results are used for visualization purpose and are not measured data points of experiments.

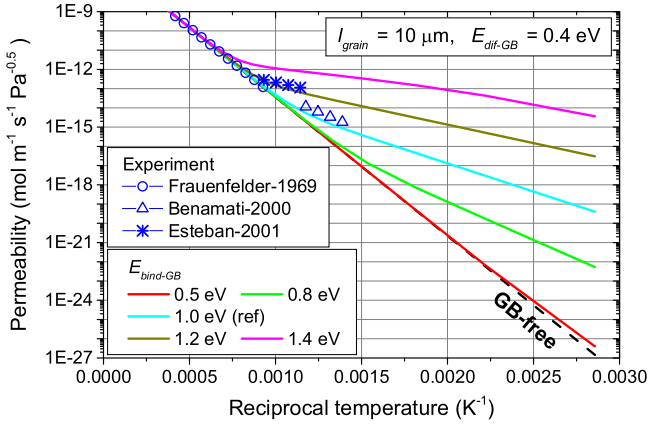

Fig. 11. Influence of the binding energy to GBs ($E_{bind\text{-}GB}$) on effective hydrogen permeability (P_{eff}).

activation energy for effective permeability may be evaluated to be smaller than 1.4 eV even at high temperatures.

Fig. 11 shows the influence of $E_{bind\text{-}GB}$ on P_{eff}. In comparison with experimental data, 1.0 eV seems to be an appropriate value for $E_{bind\text{-}GB}$. In addition, $E_{bind\text{-}GB}$ = 1.0 eV is comparable with DFT calculation results for some GBs [14–16] and is consistent with the estimate acquired in Section 3.2. $E_{bind\text{-}GB}$ should not be low like 0.5 eV and not be high like 1.4 eV, as these values cause large inconsistences with the experimental results in Fig. 11. The uncertainty in $E_{bind\text{-}GB}$ = 1.0 eV would be around ±0.2 eV at most.

The effective permeability is defined as the product of the effective solubility and the effective diffusivity. Therefore, if both effective solubility and effective diffusivity obey Arrhenius equations, the activation energy of the effective permeability is expressed as $E_{eff\text{-}P} = E_{eff\text{-}S} + E_{eff\text{-}D}$, where $E_{eff\text{-}S}$, $E_{eff\text{-}D}$ and $E_{eff\text{-}P}$ are respectively the activation energies in the effective solubility, diffusivity and permeability. Thus, in a temperature range where H atoms trapped at GBs dominantly contribute to the effective solubility and the effective diffusivity, the activation energy for the effective permeability is expected to converge to $E_{eff\text{-}P} = (E_{sol\text{-}lat} - E_{bind\text{-}GB}) + E_{dif\text{-}GB}$. Indeed, the slopes of poly-crystalline systems at sufficiently low temperatures, where H atoms at GBs govern the permeation process, correspond to $E_{eff\text{-}P} = 1.58\,\text{eV} - E_{bind\text{-}GB}$ in Fig. 11 as $E_{sol\text{-}lat}$ = 1.18 eV and $E_{dif\text{-}GB}$ = 0.4 eV in the present model.

Fig. 12 shows the influence of $E_{dif\text{-}GB}$ on P_{eff}. As discussed just above, the slopes of poly-crystalline systems correspond to

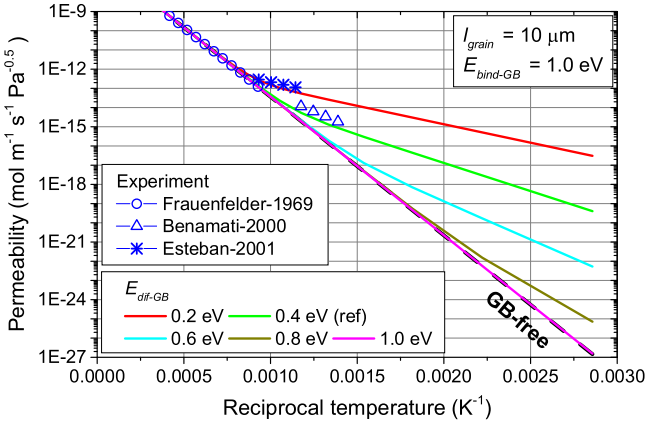

Fig. 12. Influence of the diffusion barrier along GBs ($E_{dif\text{-}GB}$) on effective hydrogen permeability (P_{eff}).

$E_{eff\text{-}P} = E_{dif\text{-}GB} + 0.18$ eV as $E_{sol\text{-}lat}$ = 1.18 eV and $E_{bind\text{-}GB}$ = 1.0 eV at sufficiently low temperatures. In comparison with experimental data, 0.4 eV seems to be appropriate for $E_{dif\text{-}GB}$. 0.2 eV is too low and 0.6 eV is too high in Fig. 12. Thus, the uncertainty in $E_{dif\text{-}GB}$ = 0.4 eV is estimated to be around ±0.1 eV.

It should be noted that, since $E_{eff\text{-}P}$ depends on both $E_{bind\text{-}GB}$ and $E_{dif\text{-}GB}$, if we set $E_{bind\text{-}GB}$ = 1.2 eV and $E_{dif\text{-}GB}$ = 0.6 eV for example, the temperature dependence of P_{eff} becomes the same with the reference case ($E_{bind\text{-}GB}$ = 1.0 eV and $E_{dif\text{-}GB}$ = 0.4 eV). Therefore, we can only determine $E_{bind\text{-}GB} - E_{dif\text{-}GB}$ value from the comparison on the effective permeability. Nevertheless, the best estimates for $E_{bind\text{-}GB}$ and $E_{dif\text{-}GB}$ at present should be 1.0 eV and 0.4 eV, respectively, because (i) the comparison results on diffusivity in Section 3.2 also suggested 0.4 eV for $E_{dif\text{-}GB}$ and (ii) 1.0 eV for $E_{bind\text{-}GB}$ is comparable with the DFT calculation results [14–16]. As discussed in this section and Section 3.2, the uncertainties in $E_{bind\text{-}GB}$ = 1.0 eV and $E_{dif\text{-}GB}$ = 0.4 eV are expected to be around ±0.2 eV and ±0.1 eV, respectively.

In Fig. 10, the model results show relatively large differences from Zakharov-1975 and Esteban-2001. The difference from Esteban-2001 is mitigated in Fig. 11 with $E_{bind\text{-}GB}$ = 1.2 eV and in Fig. 12 with $E_{dif\text{-}GB}$ = 0.2 eV. These differences are likely to result from (i) simplification and approximation adopted in the present model and (ii) the fact that GB effects are dependent on specimen or/and pretreatment. In order to reveal GB characters in practical W materials and then reveal correlation between GB characters and GB effects, systematic experimental and computational studies are needed.

3.5. *Trap effects reflected in Arrhenius plot of* P_{eff}

In experiments, P_{eff} is usually less influenced by traps than S_{eff} and D_{eff} because the effects in S_{eff} and D_{eff} can fully or partially cancel each other. In the present study, GB effects change the slope of P_{eff} at low temperatures as seen in Figs. 10–12. In this section, trap effects of lattice defects on P_{eff} in general is discussed by categorizing lattice defects into two trap types. One type is about lattice defects trapped by which H atoms cannot diffuse until detrapping, and the other type is about lattice defects trapped by which H atoms can diffuse with being trapped. The former includes vacancy, and the latter GB, surface, and probably dislocation [13]. Hereafter, the former is called Type-1 trap, and the latter Type-2 trap.

In both trap types, S_{eff}, D_{eff} and P_{eff} are expressed as follows:

$$S_{eff} = S_{H-lat} + S_{H-trap} = \left(1 + S_{H-trap}/S_{H-lat}\right) S_{H-lat} = (1+\varepsilon) S_{H-lat}, \tag{32}$$

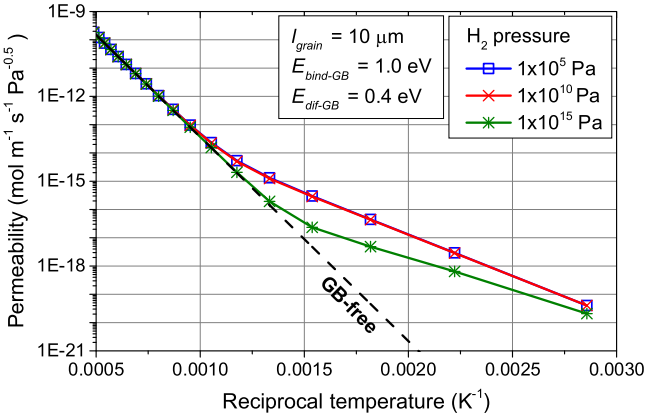

Fig. 13. Influence of H_2 partial pressure (p_{H2}) on hydrogen effective permeability (P_{eff}).

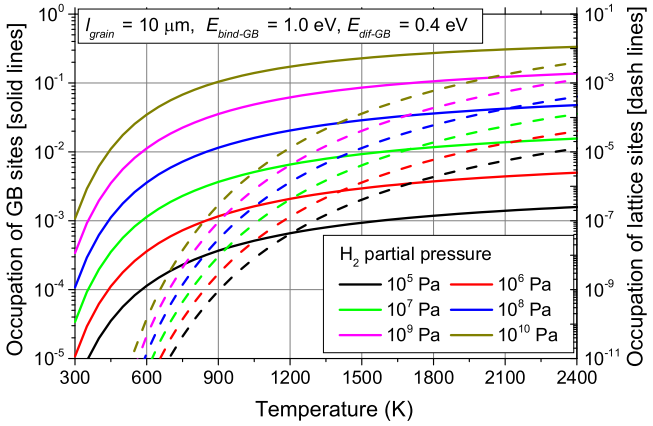

Fig. 14. Occupations of GB sites and lattice sites as functions of temperature and H_2 partial pressure.

$$D_{eff} = \left(D_{H-lat} + \varepsilon D_{H-trap}\right) / (1+\varepsilon), \tag{33}$$

$$\begin{aligned} P_{eff} &= D_{eff} S_{eff} = \left(D_{H-lat} + \varepsilon D_{H-trap}\right) S_{H-lat} \\ &= D_{H-lat} S_{H-lat} + D_{H-trap} S_{H-trap}, \end{aligned} \tag{34}$$

where $\varepsilon = S_{H\text{-}trap}/S_{H\text{-}lat}$. Therefore, in general, P_{eff} is not free from trap effects because P_{eff} is not equal to $D_{H\text{-}lat}S_{H\text{-}lat}$ in Eq. (34). Consequently, trap effects of Type-2 trap like GB are observed in P_{eff} as shown in Section 3.4.

In Type-1 trap, however, the condition $S_{H\text{-}lat}D_{H\text{-}lat} \gg S_{H\text{-}trap}D_{H\text{-}trap}$ is satisfied, as $D_{H\text{-}trap}$ is negligibly small. Indeed, a more appropriate condition to distinguish Type-1trap from Type-2 trap is whether $D_{H\text{-}trap} \ll (D_{H\text{-}lat}S_{H\text{-}trap})/S_{H\text{-}lat}$ is satisfied or not. Consequently, Eqs. (33) and (34) can be approximately rewritten for Type-1 trap as

$$D_{eff} = \left(D_{H-lat} + \varepsilon D_{H-trap}\right) / (1+\varepsilon) \sim D_{H-lat}/(1+\varepsilon), \tag{35}$$

$$\begin{aligned} P_{eff} &= D_{eff} S_{eff} \sim \left\{D_{H-lat}/(1+\varepsilon)\right\} \left\{(1+\varepsilon) S_{H-lat}\right\} \\ &= D_{H-lat} S_{H-lat} = P_{H-lat}. \end{aligned} \tag{36}$$

Eq. (36) shows that Type-1 trap does not affect P_{eff} apparently, while Type-2 trap does as shown in Eq. (34).

3.6. Pressure dependence of S_{eff}, D_{eff} and P_{eff}

The calculation results presented in Sections 3.1–3.4 were obtained with keeping the partial pressure of H_2 (p_{H2}) to be 1×10^5 Pa. Indeed, p_{H2} hardly affects S_{eff}, D_{eff} and P_{eff} unless a very large value is set. As an example, Fig. 13 shows the dependence of P_{eff} on p_{H2}. Results with p_{H2} smaller than 1×10^{10} Pa (10 GPa) are almost the same with each other. The dependence becomes clear above around 1×10^{12} Pa due to a large hydrogen occupation of GB sites, which reduces the available configuration and then makes GB sites unfavorable regarding the configurational entropy. Consequently, P_{eff} moves toward "GB-free" data to some extent at very high pressures, as seen in Fig. 13. These observations for P_{eff} are fully applicable to S_{eff} and D_{eff} as well.

Indeed, as will be explained in the next section, the present model becomes inaccurate when the pressure becomes high around 1×10^{10} Pa due to other conditions. Therefore, within conditions where the present model is accurate enough, it is reasonable to consider that P_{eff}, S_{eff} and D_{eff} are independent of p_{H2}.

3.7. Conditions where the present model appropriately works

In the present model, it is assumed that $E_{bind\text{-}GB}$ is independent of the occupation of GB sites, and then quadratic equation Eq. (14) was obtained to determine the occupation. Indeed, this assumption is appropriate in most conditions used in Chapter 3.

Fig. 14 shows the occupations of GB sites and lattice sites as a function of temperature with various H_2 partial pressures (p_{H2}). The occupation of GB sites is calculated as $f_{H\text{-}GB}N_H/N_{GB}$ and that of lattice sites as $f_{H\text{-}lat}N_H/N_L$. We may assume that the interaction between H atoms trapped by GB does not significantly occur when $f_{H\text{-}GB} < 0.125$ is satisfied, which corresponds to 1 H atom per 4 unit GB planes or less in average. This criterion relies on the fact that no H atom are trapped in neighboring unit GB planes in such a case if H atoms uniformly distribute over GB sites. Then, with this criterion, $p_{H2} < 1 \times 10^9$ Pa is the condition with which the present model appropriately works up to 2400 K. If the temperature is limited to below 1000 K, the present model works up to $p_{H2} = 1 \times 10^{10}$ Pa. If p_{H2} is higher than these pressures, it is better to consider the dependence of $E_{bind\text{-}GB}$ on the occupation of GB sites, an equation for which will be described in Appendix A.

In addition, Sieverts' law, which is used to find the equilibrium condition between H_2 molecules in the gas phase and H atoms in the lattice sites, brings some error at high pressures because H_2 gas does not behave like ideal gas. This error can be avoided by using accurate chemical potential of H_2 gas without assuming ideal gas [42] if needed, although it was not done in the present study.

4. Discussion

4.1. Uncertainties in $E_{sol\text{-}lat}$, $E_{bind\text{-}GB}$, $E_{dif\text{-}lat}$ and $E_{dif\text{-}GB}$

In Chapter 3, the comparisons with experimental results suggested that 1.0 eV and 0.4 eV are the most likely values for $E_{bind\text{-}GB}$ and $E_{dif\text{-}GB}$, respectively. The estimated uncertainties are ±0.2 eV for $E_{bind\text{-}GB}$ and ±0.1 eV for $E_{dif\text{-}GB}$, respectively. It should be recalled that $E_{bind\text{-}GB}$ is defined to be the effective value of the binding energies to various GBs. Likewise, $E_{dif\text{-}GB}$ is the effective value of the barriers of hydrogen diffusion along various GBs. Hence, if an experiment is performed with a specimen that mainly contains only a few specific GBs, $E_{bind\text{-}GB}$ and $E_{dif\text{-}GB}$ may take values away from 1.0 eV and 0.4 eV, respectively, depending on GB types [14,16,17]. Indeed, the permeability of Esteban-2001 are better reproduced with $E_{bind\text{-}GB} = 1.2$ eV than $E_{bind\text{-}GB} = 1.0$ eV, for example, as discussed in Section 3.4. In addition, since they are effective values, it is not necessarily guaranteed that their temperature dependences obey Arrhenius equation, although effective hydrogen diffusivity

Table 4
Most likely values and uncertainties for $E_{sol-lat}$, $E_{bind-GB}$, $E_{dif-lat}$ and E_{dif-GB}.

	Most likely	Lower limit	Upper limit
$E_{sol-lat}$	1.17 eV	0.98 eV	1.27 eV
$E_{bind-GB}$	1.0 eV	0.8 eV	1.2 eV
$E_{dif-lat}$	0.25 eV	0.20 eV	0.39 eV
E_{dif-GB}	0.4 eV	0.3 eV	0.5 eV

reported in a MD study obeying Arrhenius equation in GB-rich systems at 1200–2000 K [18]. Moreover, $E_{bind-GB}$ as well as E_{dif-GB} may take a different value from material to material, depending on sample pretreatment, segregation of impurities or alloy elements at GBs, etc. Further studies are needed to reveal the characteristics of $E_{bind-GB}$ and E_{dif-GB}.

There are also some uncertainties in $E_{dif-lat}$ and $E_{sol-lat}$. The most utilized $E_{dif-lat}$ is of Frauenfelder-1969, which is $E_{dif-lat}$ = 0.39 eV as in Eq. (31). Otsuka-2009, Ikeda-PDP-2011 and Ikeda-GDP-2011 reported comparable values with it. However, as suggested by Heinola et al. [35] and then confirmed with vacancy [12] and with GB in Section 3.3, it is highly possible that the two low-temperature data points in Frauenfelder-1969 were affected by traps. Then, excluding the two points, $E_{dif-lat}$ = 0.25 eV as in Eq. (23) was obtained from measured data points in Frauenfelder-1969 [35]. Moreover, the result in Section 3.2 suggested that the diffusivity of Otsuka-2009, Ikeda-PDP-2011 and Ikeda-GDP-2011 should correspond to E_{dif-GB}, not to $E_{dif-lat}$. On the other hand, DFT calculation with PBE functional [51] suggested around 0.20 ~ 0.21 eV for $E_{dif-lat}$ [10,35]. Based on all these results, it would be reasonable and safe to consider at present that 0.25 eV is the most likely value, 0.20 eV is the lower limit and 0.39 eV is the upper limit for $E_{dif-lat}$.

Regarding $E_{sol-lat}$, since the solubility is readily affected by traps, it is better to indirectly determine $E_{sol-lat}$ from $E_{perm-lat}$ and $E_{dif-lat}$ according to $E_{perm-lat} = E_{sol-lat} + E_{dif-lat}$. In permeation experiments at high temperatures, where P_{eff} is expected to converge to P_{H-lat}, the activation energies for the permeability determined in several experiments nicely agree with each other: 1.46 eV in Akiten-1967, 1.37 eV in Frauenfelder-1968, and 1.43 eV in Frauenfelder-1969. Thus, the most likely value for $E_{perm-lat}$ is 1.42 eV with the uncertainty around ±0.05 eV. In comparison with the uncertainties in $E_{dif-lat}$, it would be reasonable to consider at present that the lower limit of $E_{sol-lat}$ is 0.98 eV, which is obtained with $E_{perm-lat}$ = 1.37 eV and $E_{dif-lat}$ = 0.39 eV of Frauenfelder-1969, the higher limit is 1.27 eV, which is obtained with $E_{perm-lat}$ = 1.47 eV and $E_{dif-lat}$ = 0.20 eV of DFT calculation, and the most likely value is 1.17 eV, which is obtained with $E_{perm-lat}$ = 1.42 eV and $E_{dif-lat}$ = 0.25 eV of Heinona-2010.

Finally, it should be noted that the discussion in this section was made with assuming that the four quantities ($E_{sol-lat}$, $E_{bind-GB}$, $E_{dif-lat}$ and E_{dif-GB}) are constant and independent of experimental conditions such as temperature, hydrogen concentration, etc. If this is not the case, the uncertainties in these quantities would be larger than what was estimated in this section.

The most likely values and estimated uncertainties for $E_{sol-lat}$, $E_{bind-GB}$, $E_{dif-lat}$ and E_{dif-GB} are summarized in Table 4.

4.2. Future works to deepen the understanding of GB effects

4.2.1. Experiments to refine $E_{sol-lat}$, $E_{bind-GB}$, $E_{dif-lat}$ and E_{dif-GB}

The results of the present study can be also used to design promising experiments for deepening the understanding of the GB effects. For example, a permeability experiment with a specimen of known grain size over wide temperature range will provide nice information on $E_{bind-GB}$ and E_{dif-GB}. The slope at low temperatures converge to $(E_{sol-lat} - E_{bind-GB}) + E_{dif-GB}$, while that at high temperatures to $E_{sol-lat} + E_{dif-lat}$. It is better not to use a specimen of small grains because it blurs the boundary between the low-temperature region and the high-temperature region as shown in Fig. 10. For example, an experiment with 10 μm grain over 500–1500 K is a good condition to clearly divide the two regions and then to accurately determine the slopes.

In addition to this permeability experiment, in order to determine the four key quantities, the effective diffusivity needs to be measured with the same specimen from a low temperature at around 500 K to a high temperature like 2000 K. With this measurement, $E_{dif-lat}$ can be determined from the slope at the high-temperature region and E_{dif-GB} from the slope at the low-temperature region, as shown in Fig. 6. Then, the results of these permeation and diffusion experiments enable us to uniquely determine the four key parameters ($E_{sol-lat}$, $E_{bind-GB}$, $E_{dif-lat}$, E_{dif-GB}) for the GB effects.

4.2.2. Experiments for characterization of $E_{bind-GB}$ and E_{dif-GB}

Another important subject is to check how the hydrogen occupation of GB sites affects $E_{bind-GB}$ and E_{dif-GB}. As shown in Section 3.4, the permeability is almost independent of H_2 partial pressure unless the pressure is extremely high. This is because E_{dif-GB} and $E_{bind-GB}$ are assumed to be independent of the occupation of GB sites in the present model. Thus, if one observes a pressure dependence of the permeability with moderate pressures (lower than 1×10^{10} Pa) in experiments, this observation indicates that $E_{bind-GB}$ and/or E_{dif-GB} are dependent on the hydrogen occupation on GB sites. Experiments on the temperature dependence of the permeability also indicate us whether effective values can be defined for $E_{bind-GB}$ and E_{dif-GB}, and whether the effective values obey Arrhenius equation. We may also see such pressure and temperature dependences in S_{eff} and D_{eff} by the same reason with P_{eff}.

4.3. Implications to fusion engineering R&D

In fusion engineering, the effective solubility is relevant with tritium inventory and the effective permeability with tritium leakage in/from reactor materials. Hence, it is important to know how GBs affect these quantities for fuel cycle sustainability and radiation safety, which is the motivation of the present study. If a fine-grain material whose grain size is around 0.01–0.1 μm is utilized in fusion reactors, the effective solubility and permeability become 10^3–10^2 times as large as those of normal grain materials (l_{grain} = 10 μm for example) without including effects of other traps than GBs. In developing fine-grain materials, this point needs to be carefully considered, although effects of radiation damages would overwhelm the GB effects in the fusion reactor environment. If the increases in the inventory and the leakage are beyond an acceptable level, some engineering measures to decrease $E_{bind-GB}$ or/and to increase E_{dif-GB} are needed. The former measure basically reduces S_{eff} and P_{eff}, while the latter D_{eff} and P_{eff}.

Finally, it should be noticed that the effective solubility might be underestimated in experiments if it is measured after stopping hydrogen gas/plasma exposure, not during the exposure. This is because H atoms trapped by GBs are mobile enough to diffuse out to the surface even at room temperature and then a certain portion of them may be released before the solubility measurement. This point should be paid attention to not only for GB but also for other defects like dislocation, namely for some of Type-2 traps defined in Section 3.5.

5. Conclusion

In the present study, a thermodynamic model to evaluate effects of grain boundary (GB) on hydrogen behaviors in poly-crystalline W was established based on the equilibrium theory. With this model, the effective solubility, diffusivity and permeability of hydrogen

in W equilibrated with surrounding H_2 gas can be calculated as a function of grain size, temperature and H_2 partial pressure.

By setting 1.0 eV to the binding energy of hydrogen to GBs ($E_{bind\text{-}GB}$) and 0.4 eV to the diffusion barrier of hydrogen along GBs ($E_{dif\text{-}GB}$), the model reasonably reproduces experimental data on the effective diffusivity and permeability. These values ($E_{bind\text{-}GB}$ = 1.0 eV and $E_{dif\text{-}GB}$ = 0.4 eV) fairly agree with results obtained by atomistic simulations in previous studies. The uncertainties in the values were estimated to be around ±0.2 eV for $E_{bind\text{-}GB}$ and ±0.1 eV for $E_{dif\text{-}GB}$, respectively, in comparison with available experimental results.

Throughout the present study, it was confirmed that GBs significantly affect the hydrogen behaviors up to around 1000 K or higher in practical materials. Hence, the effects of GBs should be considered in analysis of experimental results and in prediction of tritium inventory and leakage in fusion reactors. Particularly for fine-grain materials, close attention needs to be paid to possible increases in the effective solubility and permeability.

The thermodynamic model constructed in the present study are expected to help analyze experimental data and then uncover GB effects. In order to facilitate the use of the present thermodynamic model, approximate equations to easily calculate the effective solubility, diffusivity and permeability in poly-crystalline W are also presented in Appendix B.

Acknowledgements

This research was supported by National Research Foundation (NRF) of Korea under Nuclear Fusion Basic Research program. The computer simulation was performed using supercomputers and technical support provided by the National Institute of Supercomputing and Network at the Korea Institute of Science and Technology Information (Project-ID: KSC-2014-C1-046). This research was also supported by BK 21 plus project and by the Center for Advanced Research in Fusion Reactor Engineering (CARFRE) in Seoul National University.

Appendix A. Model with binding energy depending on the occupation of GB sites

In Section 2.3, it was assumed that the binding energy to GB is independent of the number of trapped H atoms. This means that $E_{bind\text{-}GB}$ is not a function of xN_H/N_{GB} but a constant. xN_H/N_{GB} corresponds to hydrogen occupation of GB sites. Here, we derive an equation to determine x with a binding energy depending on the occupation.

By defining $E_{bind\text{-}GB}$ as a function of xN_H/N_{GB}, Eq. (13) is altered to be

$$\frac{\partial A}{\partial x} = N_H \left\{ -E_{bind-GB} - \frac{xN_H}{N_{GB}} \frac{dE_{bind-GB}}{dx} - k_B T \ln \left\{ \frac{(1-x)(N_{GB}-xN_H)}{x(N_L-(1-x)N_H)} \right\} \right\} = 0.$$

This equation is converted to the following quadratic equation regarding x:

$$ax^2 + bx + c = 0, \tag{A.2}$$

$$a = \frac{-N_L \exp\left(-E_{bind-GB}/k_B T\right) - N_{GB}}{N_H(1-c)} - 1, \tag{A.3}$$

$$b = \frac{N_{GB}}{N_H(1-c)}, \tag{A.4}$$

$$c = \exp\left(\frac{-E_{bind-GB} - \left(xN_H/N_{GB}\right)\left(dE_{bind-GB}/dx\right)}{k_B T} \right). \tag{A.5}$$

One of two roots of the quadratic equation that holds a value between 0 and 1 is what we look for here. However, since c contains x, this problem cannot be analytically solved. Instead, this problem requires numerical solution using an iteration method. Specifically, after obtaining an initial guess of x using Eq. (14), c is determined with Eq. (A.5) and then x is updated by solving Eq. (A.2) with the determined c. This updated x is put into Eq. (A.5) to update c. This process to update x and c will be repeated until a required consistency between the current x and the updated x is achieved.

Appendix B. Simplified equations for easy estimation of GB effects

In Eq. (13), if $(1-x)N_H/N_L \ll 1$ is further satisfied in addition to $xN_H/N_{GB} \ll 1$, the equilibrium condition is expressed by the following equation:

$$\frac{\partial A}{\partial x} \sim N_H \left\{ -E_{bind-GB} - k_B T \ln \left\{ \frac{(1-x)N_{GB}}{xN_L} \right\} \right\} = 0. \tag{B.1}$$

This equation gives us a simple expression of x as follows:

$$x \sim \frac{N_{GB}}{N_L \exp -E_{bind-GB}/RT + N_{GB}}. \tag{B.2}$$

Indeed, Eq. (B.2) largely simplifies the evaluation of GB effects on S_{eff}, D_{eff} and P_{eff} without reducing the accuracy in most conditions because $(1-x)N_H/N_L \ll 1$ is usually satisfied in W. Note that $(1-x)N_H/N_L$ corresponds to the occupation of the lattice sites and xN_H/N_{GB} to the occupation of the GB sites.

In most of normal conditions, for example all conditions used in Figs. 3–12, both $xN_H/N_{GB} \ll 1$ and $(1-x)N_H/N_L \ll 1$ are satisfied as shown in Fig. 14. Then, Eq. (B.2) becomes a nice approximation for x. With Eq. (B.2), S_{eff}, D_{eff} and P_{eff} are analytically expressed as functions of grain size (l_{grain}), temperature (T), H_2 partial pressure (p_{H2}) and some other parameters defined in Chapter 2 as follows:

$$\begin{aligned} f_{H-GB} = x &= \frac{N_{GB}}{N_{GB} + N_L \exp\left(-E_{bind-GB}/RT\right)} \\ &= \frac{3\beta l_{lat}}{3\beta l_{lat} + \alpha l_{grain} \exp\left(-E_{bind-GB}/RT\right)}, \end{aligned} \tag{B.3}$$

$$\begin{aligned} f_{H-lat} = 1 - f_{H-GB} &= \frac{N_L \exp\left(-E_{bind-GB}/RT\right)}{N_{GB} + N_L \exp\left(-E_{bind-GB}/RT\right)} \\ &= \frac{\alpha l_{grain} \exp\left(-E_{bind-GB}/RT\right)}{3\beta l_{lat} + \alpha l_{grain} \exp\left(-E_{bind-GB}/RT\right)}, \end{aligned} \tag{B.4}$$

$$\begin{aligned} S_{eff} &= \frac{1}{1-f_{H-GB}} \times S_{H-lat} \\ &= \left\{ 1 + \frac{3\beta l_{lat}}{\alpha l_{grain} \exp\left(-E_{bind-GB}/RT\right)} \right\} \times S_{H-lat}, \end{aligned} \tag{B.5}$$

$$\begin{aligned} D_{eff} = f_{H-lat} D_{H-lat} + f_{H-GB} D_{H-GB} &= \frac{\left\{ \alpha l_{grain} \exp\left(-E_{bind-GB}/RT\right) \right\} D_{H-lat} + 3\beta l_{lat} D_{H-GB}}{3\beta l_{lat} + \alpha l_{grain} \exp\left(-E_{bind-GB}/RT\right)} \\ &= \left\{ 1 + \frac{3\beta l_{lat} \left(\left(D_{H-GB}/D_{H-lat}\right) - 1 \right)}{3\beta l_{lat} + \alpha l_{grain} \exp\left(-E_{bind-GB}/RT\right)} \right\} \times D_{H-lat} \end{aligned}, \tag{B.6}$$

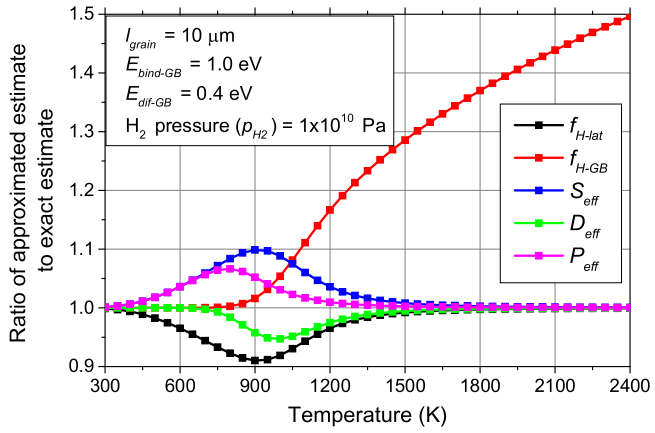

Fig. B1. Errors induced by the approximation in Appendix B as a function of temperature.

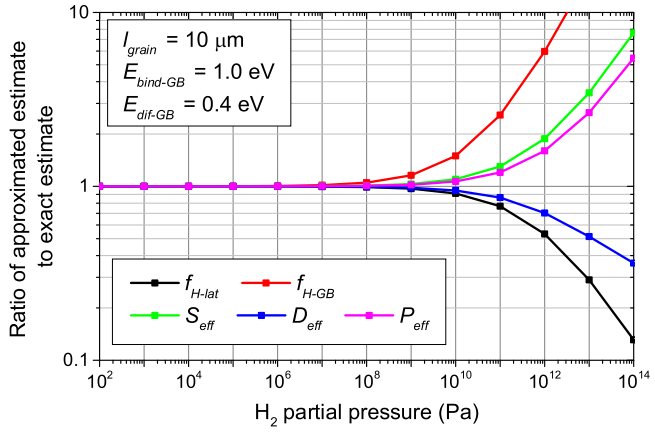

Fig. B2. Errors induced by the approximation in Appendix B as a function of H_2 partial pressure (p_{H2}).

$$P_{eff} = S_{eff}D_{eff} = \left\{1 + \frac{3\beta l_{lat}\left(D_{H-GB}/D_{H-lat}\right)}{\alpha l_{grain}\exp\left(-E_{bind-GB}/RT\right)}\right\} \times S_{H-lat}D_{H-lat}$$
$$= \left\{1 + \frac{3\beta l_{lat}\left(D_{H-GB}/D_{H-lat}\right)}{\alpha l_{grain}\exp\left(-E_{bind-GB}/RT\right)}\right\} \times P_{H-lat} \quad \text{(B.7)}$$

The accuracy of Eqs. (B.2)–(B.7) is verified in Figs. B1 and B2. The y-axes of these figures are the ratio of calculation results approximately obtained with Eq. (B.2), which is named "approximated estimate", to calculation results exactly obtained with Eq. (14), which is named "exact estimate". This ratio indicates an error caused by Eqs. (B.2)–(B.7). The ratios on $f_{H\text{-}lat}$, $f_{H\text{-}GB}$, S_{eff}, D_{eff} and P_{eff} are presented as a function of temperature in Fig. B1 and as a function of H_2 partial pressure in Fig. B2.

As shown in Fig. B1 with $p_{H2} = 1 \times 10^{10}$ Pa, the error in x (and thus in $f_{H\text{-}GB}$) is enlarged at high temperatures. This is because the condition $(1-x)N_H/N_L \ll 1$ becomes unsatisfactory at high temperatures with a large p_{H2}, as clearly seen in Fig. 14. The errors in S_{eff}, D_{eff} and P_{eff} are usually smaller than that in $f_{H\text{-}GB}$.

The ratio given in Fig. B2 is the one that holds the maximum absolute value in log([*exact estimate*]/[*approximated estimate*]) over tested temperatures, from 300 K to 2400 K with 50 K interval. The logarithm value indicates the degree of deviation from the exact estimate. The deviation is maximized at around 700–1250 K for $f_{H\text{-}lat}$, S_{eff}, D_{eff} and P_{eff}, while at 2400 K for $f_{H\text{-}GB}$. Up to around $p_{H2} = 1 \times 10^9$ Pa, the errors caused by the approximation are only around 3% at most in S_{eff}, D_{eff} and P_{eff} in the reference case. The errors increase to around 10% with $p_{H2} = 1 \times 10^{10}$ Pa, excluding larger errors in $f_{H\text{-}GB}$, as shown in Fig. B2.

As discussed in Section 3.7, the present model itself cannot work appropriately if p_{H2} is larger than around 1×10^{10} Pa. Therefore, within the conditions with which the present model is expected to work well, using Eq. (B.2) instead of the solution of Eq. (14) is reasonably accurate. For analysis of experimental results, therefore, Eqs. (B.3)–(B.7) are convenient equations to estimate GB effects in S_{eff}, D_{eff} and P_{eff}.

References

[1] T. Tanabe, Phys. Scr. T159 (2014) 014044.
[2] G.-H. Lu, H.-B. Zhou, C.S. Becquart, Nucl. Fusion 54 (2014) 086001.
[3] M. Shimada, Y. Hatano, P. Calderoni, T. Oda, Y. Oya, M. Sokolov, K. Zhang, G. Cao, R. Kolasinski, J.P. Sharpe, J. Nucl. Mater. 415 (2011) S667.
[4] Y. Hatano, M. Shimada, T. Otsuka, Y. Oya, V.K. Alimov, M. Hara, J. Shi, M. Kobayashi, T. Oda, G. Cao, K. Okuno, T. Tanaka, K. Sugiyama, J. Roth, B. Tyburska-Püschel, J. Dorner, N. Yoshida, N. Futagami, H. Watanabe, M. Hatakeyama, H. Kurishita, M. Sokolov, Y. Katoh, Nucl. Fusion 53 (2013) 073006.
[5] K. Ohsawa, J. Goto, M. Yamakami, M. Yamaguchi, M. Yagi, Phys. Rev. B 82 (2010) 184117.
[6] K. Heinola, T. Ahlgren, K. Nordlund, J. Keinonen, Phys. Rev. B 82 (2010) 094102.
[7] D.F. Johnson, E.A. Carter, J. Mater. Res. 25 (2011) 315.
[8] X.-S. Kong, S. Wang, X. Wu, Y.-W. You, C.S. Liu, Q.F. Fang, J.-L. Chen, G.-N. Luo, Acta Mater. 84 (2015) 426.
[9] Y.-W. You, X.-S. Kong, X.-B. Wu, Y.-C. Xu, Q.F. Fang, J.L. Chen, G.-N. Luo, C.S. Liu, B.C. Pan, Z. Wang, AIP Adv. 3 (2013) 012118.
[10] N. Fernandez, Y. Ferro, D. Kato, Acta Mater. 94 (2015) 307.
[11] K. Schmid, U. von Toussaint, T. Schwarz-Selinger, J. Appl. Phys. 116 (2014) 134901.
[12] T. Oda, D. Zhu, Y. Watanabe, J. Nucl. Mater. 467 (2015) 439.
[13] D. Terentyev, V. Dubinko, A. Bakaev, Y. Zayachuk, W. Van Renterghem, P. Grigorev, Nucl. Fusion 54 (2014) 042004.
[14] H.-B. Zhou, Y.-L. Liu, S. Jin, Y. Zhang, G.-N. Luo, G.-H. Lu, Nucl. Fusion 50 (2010) 025016.
[15] W. Xiao, W.T. Geng, J. Nucl. Mater. 430 (2012) 132.
[16] C. González, M. Panizo-Laiz, N. Gordillo, C.L. Guerrero, E. Tejado, F. Munnik, P. Piaggi, E. Bringa, R. Iglesias, J.M. Perlado, R. González-Arrabal, Nucl. Fusion 55 (2015) 113009.
[17] U. von Toussaint, S. Gori, A. Manhard, T. Höschen, C. Höschen, Phys. Scr. T145 (2011) 014036.
[18] P.M. Piaggi, E.M. Bringa, R.C. Pasianot, N. Gordillo, M. Panizo-Laiz, J. del Río, C. Gómez de Castro, R. Gonzalez-Arrabal, J. Nucl. Mater. 458 (2015) 233.
[19] Y. Yu, X. Shu, Y.-N. Liu, G.-H. Lu, J. Nucl. Mater. 455 (2014) 91.
[20] X.S. Kong, Y.W. You, Q.F. Fang, C.S. Liu, J.L. Chen, G.N. Luo, B.C. Pan, Z. Wang, J. Nucl. Mater. 433 (2013) 357.
[21] C.S. Becquart, C. Domain, J. Nucl. Mater. 386–388 (2009) 109.
[22] K. Heinola, T. Ahlgren, J. Nucl. Mater. 438 (2013) S1001.
[23] O. Ogorodnikova, J. Roth, M. Mayer, J. Nucl. Mater. 313–316 (2003) 469.
[24] H. Kurishita, Y. Amano, S. Kobayashi, K. Nakai, H. Arakawa, Y. Hiraoka, T. Takida, K. Takebe, H. Matsui, J. Nucl. Mater. 367–370 (2007) 1453.
[25] H. Kurishita, H. Arakawa, S. Matsuo, T. Sakamoto, S. Kobayashi, K. Nakai, G. Pintsuk, J. Linke, S. Tsurekawa, V. Yardley, K. Tokunaga, T. Takida, M. Katoh, A. Ikegaya, Y. Ueda, M. Kawai, N. Yoshida, Mater. Trans. 54 (2013) 456.
[26] N. Juslin, P. Erhart, P. Träskelin, J. Nord, K.O.E. Henriksson, K. Nordlund, E. Salonen, K. Albe, J. Appl. Phys. 98 (2005) 123520.
[27] X.-C. Li, X. Shu, Y.-N. Liu, F. Gao, G.-H. Lu, J. Nucl. Mater. 408 (2011) 12.
[28] Y.A. Du, J. Rogal, R. Drautz, Phys. Rev. B 86 (2012) 174110.
[29] K.-D. Rasch, R.W. Siegel, H. Schultz, Philos. Mag. A 41 (1980) 91.
[30] D. Kato, H. Iwakiri, K. Morishita, J. Plasma Fusion Res. Ser. 8 (2009) 404.
[31] D. Zhu, T. Oda, J. Nucl. Mater. 469 (2016) 237.
[32] M. Fukumoto, H. Kashiwagi, Y. Ohtsuka, Y. Ueda, M. Taniguchi, T. Inoue, K. Sakamoto, J. Yagyu, T. Arai, I. Takagi, T. Kawamura, J. Nucl. Mater. 390–391 (2009) 572.
[33] M. Shimada, G. Cao, Y. Hatano, T. Oda, Y. Oya, M. Hara, P. Calderoni, Phys. Scr. T145 (2011) 014051.
[34] R. Frauenfelder, J. Vac. Sci. Technol. 6 (1969) 388.
[35] K. Heinola, T. Ahlgren, J. Appl. Phys. 107 (2010) 113531.
[36] K. Heinola, T. Ahlgren, Phys. Rev. B 81 (2010) 073409.
[37] P. Alnot, A. Cassuto, D.A. King, Surf. Sci. 215 (1989) 29.
[38] S. Markelj, O.V. Ogorodnikova, P. Pelicon, T. Schwarz-Selinger, I. Čadež, Appl. Surf. Sci. 282 (2013) 478.
[39] R. Frauenfelder, J. Chem. Phys. 48 (1968) 3955.
[40] G. Benamati, E. Serra, C. Wu, J. Nucl. Mater. 283–287 (2000) 1033.
[41] H. Nakamura, W. Shu, T. Hayashi, M. Nishi, J. Nucl. Mater. 313–316 (2003) 679.

[42] Y. Fukai, The Metal-Hydrogen System, Springer-Verlag, Berlin/Heidelberg, 2005.
[43] A.P. Zakharov, V.M. Sharapov, E.I. Evko, Sov. Mater. Sci. 9 (1975) 149.
[44] G.A. Esteban, A. Perujo, L.A. Sedano, K. Douglas, J. Nucl. Mater. 295 (2001) 49.
[45] T. Otsuka, T. Hoshihira, T. Tanabe, Phys. Scr. T138 (2009) 014052.
[46] Y.M. Gasparyan, A.V. Golubeva, M. Mayer, A.A. Pisarev, J. Roth, J. Nucl. Mater. 390–391 (2009) 606.
[47] T. Ikeda, T. Otsuka, T. Tanabe, Fusion Sci. Technol. 60 (2011) 1463.
[48] T. Ikeda, T. Otsuka, T. Tanabe, J. Nucl. Mater. 415 (2011) S684.
[49] E.A. Aitken, H.C. Brassfield, P.K. Conn, E.C. Duderstadt, R.E. Fryxell, Trans. Metall. Soc. AIME 239 (1967) 1565.
[50] S.A. Steward, Review of Hydrogen Isotope Permeability through Materials, Livermore, CA, 1983.
[51] J.P. Perdew, K. Burke, M. Ernzerhof, Phys. Rev. Lett. 77 (1996) 3865.